7-1-2020

CD4 Deficiency Causes Poliomyelitis and Axonal Blebbing in Murine Coronavirus-Induced Neuroinflammation.

Debanjana Chakravarty
Indian Institute of Science Education and Research

Fareeha Saadi
Indian Institute of Science Education and Research

Soumya Kundu
Indian Institute of Science Education and Research

Abhishek Bose
Indian Institute of Science Education and Research

Reas Khan
University of Pennsylvania Scheie Eye Institute

See next page for additional authors

CD4 deficiency causes poliomyelitis and axonal blebbing in murine coronavirus induced neuroinflammation

Running title: CD4 T cells prevent poliomyelitis and axonal dystrophy

Debanjana Chakravarty[1#], Fareeha Saadi[1#], Soumya Kundu[1], Abhishek Bose[1], Reas Khan[2], Kimberly Dine[2], Lawrence C Kenyon[3], Kenneth S Shindler[2,4*] and Jayasri Das Sarma[1,*]

[1]Department of Biological Sciences, Indian Institute of Science Education and Research Kolkata, Mohanpur-741246, India

[2]Departments of Ophthalmology and[4] Neurology University of Pennsylvania Scheie Eye Institute, Philadelphia, PA 19104, USA

[3]Department of Pathology, Anatomy and Cell Biology, Thomas Jefferson University, Philadelphia, PA 19107, USA

ABSTRACT:

Mouse hepatitis virus (MHV) is a murine β-coronavirus (m-CoV) which causes a wide range of diseases in mouse and rat, including hepatitis, enteritis, respiratory diseases, and encephalomyelitis in the CNS. MHV infection in mice provides an efficient cause-effect experimental model to understand the mechanisms of direct virus induced neural cell damage leading to demyelination and axonal loss which are pathological features of Multiple sclerosis (MS), the most common disabling neurological disease in young adults. Infiltration of T lymphocytes, activation of microglia and their interplay are the primary pathophysiological events leading to the disruption of myelin sheath in MS. However, there are emerging evidences supporting gray matter involvement and degeneration in MS. The investigation of T cell function in the pathogenesis of deep gray matter damage is necessary. Here, we employed RSA59 (isogenic recombinant strain of MHV-A59) induced experimental neuroinflammation model to compare the disease in $CD4^{-/-}$ mice with $CD4^{+/+}$ mice at days 5, 10, 15, and 30 p.i. Viral titer estimation, nucleocapsid gene amplification and viral anti-nucleocapsid staining confirm enhanced replication of the virions in the absence of functional $CD4^{+}$ T cells in the brain. Histopathological analyses showed an elevated susceptibility of $CD4^{-/-}$ mice to axonal degeneration in the CNS with augmented progression of acute poliomyelitis, and dorsal root ganglionic inflammation rarely observed in $CD4^{+/+}$ mice. Depletion of $CD4^{+}$ T cells shows unique pathological bulbar vacuolation in the brain parenchyma of infected mice with persistent CD11b+ microglia/macrophages in the inflamed regions on day 30 p.i. In summary,

the current study suggests that $CD4^+$ T cells are critical for controlling acute stage poliomyelitis (gray matter inflammation) and chronic axonal degeneration, inflammatory demyelination due to loss of protective anti-viral host immunity.

#: Equal contribution

Debanjana Chakravarty and Fareeha Saadi contributed equally to this work. Author order was determined based on the relatedness of the work with Debanjana Chakravarty's PhD thesis.

*** Corresponding authors:**

Kenneth S. Shindler: Departments of Ophthalmology and Neurology, University of Pennsylvania, Scheie Eye Institute, Philadelphia, PA 19104, USA. E-mail: Kenneth.Shindler@uphs.upenn.edu

Jayasri Das Sarma**:** Department of Biological Sciences, Indian Institute of Science Education and Research Kolkata, Mohanpur-741246, India. E-mail: dassarmaj@iiserkol.ac.in

KEYWORDS: $CD4^+$T cells, Microglia, MHV infection, mCoV, Neuroinflammation, Innate immune response, Demyelination, Host Immunity

IMPORTANCE

The current trend in CNS disease biology is to understand the neural cell-immune interaction to investigate the underlying mechanism of neuroinflammation, rather than focusing on peripheral immune activation. Most studies in MS are targeted toward understanding the involvement of CNS white matter. However, the importance of gray matter damage has become critical in understanding the long-term progressive neurological disorder. Our study highlights the importance of $CD4^+$T cells in safeguarding the neurons against axonal blebbing and poliomyelitis from murine Betacoronavirus-induced neuroinflammation. Current knowledge of the mechanisms that lead to gray matter damage in MS is limited, because the most widely used animal model EAE does not present this aspect of the disease. Our results thus, add to the existing limited knowledge in the field. We also show that the microglia, though important for the initiation of neuroinflammation, cannot establish a protective host immune response without the help of $CD4^+$ T cells.

INTRODUCTION

Neuroinflammation is the cardinal signature of several complex and multi-faceted central nervous system (CNS) disorders. CNS inflammation is known to be initiated mainly by the brain's resident innate immune cells, the microglia, which rapidly respond to an infectious agent or any perturbation in the CNS. Via the secretion of chemokines and cytokines, they direct the extravasation of several myeloid cells, including neutrophils, monocytes/macrophages, and dendritic cells, which in turn promote the entry and activation of adaptive immune responsive T cell populations into the CNS(1-4).

Regulation of T cells is central to understanding the cellular and humoral immunity in neuroinflammation. So far, most studies have demonstrated the destructive pathogenic effects of encephalitogenic T cells in neurodegeneration. For example, Multiple sclerosis (MS the most common neurological disease of young adults is characterized predominantly by self-reactive myelinolytic T cell-mediated autoimmune destruction of the myelin sheath (5-10). Likewise, in an experimental animal model of MS, Experimental autoimmune encephalomyelitis (EAE), the disease mainly depends on the infiltration of pathogenic $CD4^+$ T cells, which are primarily of Th1 and Th17 types (11-19). Studies have also shown a pathogenic role of myelin-specific $CD8^+$ T cells in the inflammatory lesions in EAE mice brains (20-22). A Mouse hepatitis virus (MHV) (V5A13.1) model of induced neuroinflammation showed a significant reduction in the severity of inflammation and demyelination in $CD4^{-/-}$ mice at days 12-21 p.i. compared to both $CD8^{-/-}$ and wild type mice (23). Adoptive transfer of $CD4^+$T cells and $CD8^+$T enriched splenocytes differentially affect the state of inflammation and demyelination in MHV-JHM infected $RAG^{-/-}$ mice and induction of donor splenocytes with a depleted population of both CD4 and $CD8^+$ T cells in JHM infected $RAG^{-/-}$ mice prevents demyelination (24). However, recent advances have shown that the prevalence of activated adaptive immune responses are not restricted to neuroinflammatory myelin degeneration as seen in MS but translates across classic neurodegenerative disorders such as Alzheimer's disease (AD), Parkinson's disease (PD) and Amyotrophic lateral sclerosis (ALS) (25, 26) (27, 28) (29) (30).

With the shift in the paradigm of CNS immunology and the discovery of CNS meningeal lymphatic vessels, several studies also suggested that $CD4^+$ T cells may provide protective immunity against cognitive and motor disabilities in neurodegenerative disorders (31) (32). Activated $CD4^+$ T cells also help in limiting MHV-JHM replication within the CNS (33). Either CD4 or CD8 deletion in Theiler's Murine Encephalomyelitis (TMEV) resistant B6 strain

makes the mice susceptible to disease and shows increased viral persistence and demyelination (34). The current research trend is thus targeted toward understanding the differential mechanisms that regulate the balance between neuroprotection and neurodestruction conferred by $CD4^+$ T cells.

Several studies have demonstrated the accumulation of microglia/macrophages in the vicinity of reactive $CD4^+$ T cells in CNS lesions during neurodegeneration (4, 30, 35-37). While ample literature supports $CD4^+$ T cells interaction with CNS resident microglia and/or infiltrating myeloid-specific monocytes/macrophages as the primary mechanisms underlying white matter damage in the early relapsing-remitting stage of MS, one cannot overlook their function behind immune mediated greay matter atrophy.

The current study is focused on understanding the potential protective role of $CD4^+$ T cells on microglial activation and their cooperative effect on both white and gray matter damage following infection with a neurotropic isogenic spike protein recombinant strain of Betacoronavirus MHV, RSA59. Intracranial infection of C57BL/6 mice with RSA59 results in a biphasic disease, characterized by acute hepatitis and meningoencephalomyelitis followed by chronic immune-mediated demyelination and concomitant axonal loss, which mimics specific pathologies of the human demyelinating disease MS (38-40). RSA59 induced acute neuroinflammation comprises mixed populations of astrocytes and inflammatory cells, mainly microglia/macrophages and a smaller population of T lymphocytes (40-44). As early as day 3 post-infection (p.i.), peripheral leukocytes start to infiltrate the CNS, beginning with the cells of the innate immune response predominantly myeloid cells such as neutrophils and monocytes/macrophages. Lymphoid cells, including CD4, CD8, and NK T cells start to appear in the CNS at day 5 p.i. and their infiltration peaks at day 7 p.i. followed by the start of viral clearance (Fig. 1). While $CD8^+$ T cells begin to disappear as early as day 10 p.i. and NK T cells reduce in number, a significant number of $CD4^+$ T cells are present in the inflamed brain even at day 16 p.i. (Fig. 1). While inflammation resolves and infectious virus particles clear from the brain, Iba1+ macrophages/microglia persist significantly within the demyelinating plaques in the spinal cord white matter and are known to cause direct myelin stripping (40). Recent Affymetrix microarray analysis in the spinal cord of RSA59 infected mice showed elevated expression of inflammatory mediators during the acute stage of infection. Interestingly, conventional T and B cell markers showed no or insignificant upregulation (45, 46). Expression of adaptive immune responsive genes showed prominent upregulation during the chronic phase

(46). The most striking associations were observed between CD3, CD45, and MHCII expression, which promote the communication between innate and adaptive immune systems via microglia-$CD4^{+}$T cell signalling.

Current study employs a CD4 knock out strain in the background of C57BL/6 mice ($CD4^{-/-}$). In comparison to the wild type C57BL/6 mice ($CD4^{+/+}$), infection of $CD4^{-/-}$ mice produces an exaggerated disease course in association with enhanced viral replication and prolonged viral persistence. Moreover, $CD4^{-/-}$ mice are more susceptible to chronic inflammation, and axonal degeneration compared to $CD4^{+/+}$ mice, and CD11b+ macrophages/microglia show persistent activation even during the chronic disease phase. Our results suggest a novel neuroprotective role of $CD4^{+}$ T cells in the MHV induced demyelinating model of MS unlike the EAE model where T cells have a predominantly pathogenic role.

RESULTS

Mice were inoculated with isogenic EGFP expressing RSA59 as described in the materials and methods section. Experimental mice were monitored daily for the development of clinical signs and symptoms. The majority of $CD4^{+/+}$ mice displayed low disease scores ranging from 0.5 to 1, indicated by ruffled fur and occasionally present the hunch back phenotype as observed previously (47). 100 % mice survived until day 30 p.i as observed . Though not significantly different, $CD4^{-/-}$ mice showed a slightly higher disease score of 1.5 to 2 indicated by hind limb weakness in addition to hunch back, the symptoms started appearing as early as day 3-5 p.i., however, almost 90% mice survived until day 30 p.i. The scoring system has been discussed in the materials and methods section.

The absence of functional $CD4^{+}$ T cells does not alter acute stage hepatitis and meningoencephalomyelitis but shows gray matter involvement in the form of poliomyelitis and Dorsal Root Ganglion inflammation.

The current study initially investigated differences in phenotypic or pathological symptoms as well as basal level of inflammation at the tissue level between mock infected $CD4^{+/+}$ and $CD4^{-/-}$ mice. No significant differences were observed at the phenotypic level. Conventional light microscopy data analysis at H& E staining sections from liver, brain and spinal cord revealed that mock infected (MI) $CD4^{+/+}$ and $CD4^{-/-}$ mice presented only a basal level of inflammation (if any) in all the three tissue types (Fig 2). Mock infected $CD4^{-/-}$ mice did not show any

differential phenotypic or histopathological features concerned for this study. All experiments were conducted using age matched $CD4^{+/+}$ and $CD4^{-/-}$ mice.

To examine the degree of inflammation in CNS and non-CNS tissues, MI and infected $CD4^{+/+}$ and $CD4^{-/-}$ mice were sacrificed at two-time points, day 5-6 p.i. (onset of the peak of neuroinflammation) and day 30 p.i. (chronic phase of inflammation). The liver, brain, and spinal cord tissues were harvested and fixed in 4 % paraformaldehyde and paraffin embedded.

During the acute phase of infection, comparable, multiple foci of moderate to severe necrotizing, and non-necrotizing hepatitis were observed in both $CD4^{+/+}$ and $CD4^{-/-}$ mice (Fig. 3a). During the chronic phase, hepatitis nearly resolved, but the number of remnant hepatic lesions were more in $CD4^{-/-}$ mice (Fig. 3b). The Hepatic Activity Index showed no significant difference at day 6 and 30 p.i. between $CD4^{+/+}$ and $CD4^{-/-}$ mice (Fig. 3b).

H&E stained brain sections from RSA59 infected $CD4^{+/+}$ and $CD4^{-/-}$ (Fig. 4a) mice demonstrated focal acute encephalitis, meningitis, intra-parenchymal perivascular lymphocytic cuffing, and microglial nodule formation at the acute phase of infection. Corresponding serial brain sections immunohistochemically stained with anti-CD45 (leukocyte common antigen, LCA) confirmed similar levels of inflammatory cells in the brain parenchyma of $CD4^{+/+}$ (2.691 ± 0.4561) and $CD4^{-/-}$ (2.485 ± 0.3849) mice(48). H&E staining of both $CD4^{+/+}$ and $CD4^{-/-}$ (Fig. 4b) infected spinal cords showed myelitis. Quantification of the staining intensity suggests that corresponding regions were equally immunoreactive for CD45, indicating the comparable infiltration of mononuclear cells in $CD4^{+/+}$ (1.176 ± 0.1958) and $CD4^{-/-}$ mice (1.355 ± 0.1947). However, the consequent anti-CD11b (pan-macrophage marker) immunohistochemistry revealed significantly fewer macrophage/microglia in the brains and spinal cords of $CD4^{-/-}$ mice (0.6067± 0.1260, ****$p<0.0001$ and 0.258 ± 0.07078, **$p<0.01$ respectively), as compared to $CD4^{+/+}$ mice (4.749 ± 0.3981, and 1.110 ± 0.3007, respectively) (Fig. 5). Moreover, apart from the white matter myelitis in both infected $CD4^{+/+}$ and $CD4^{-/-}$ mice, $CD4^{-/-}$ mice showed evidence of acute poliomyelitis (gray matter inflammation) and dorsal root ganglionic inflammation which were rarely observed in $CD4^{+/+}$ mice at the acute phase of infection (Fig. 6). Average inflammation scores,based on H&E, are shown in Table I and II.

The absence of $CD4^{+}$ T cells impairs RSA59 clearance from the brain tissue.

To assess the role of $CD4^+$ T cells in virus clearance, viral titer, viral nucleocapsid gene amplification, in situ viral antigen distribution and mRNA level of anti-viral pro-inflammatory cytokines /chemokines were evaluated.

RSA59 titer kinetics was compared in the brains of $CD4^{-/-}$ and $CD4^{+/+}$ mice, and the values were expressed as $\log_{10}$ PFU/ gram of tissue. In both mouse strains, the virus replicated efficiently in the brain at day 5 p.i. ($10^{5.8}$ PFU/gm in $CD4^{-/-}$ versus $10^{6.1}$ PFU/gm in $CD4^{+/+}$). By day 10 p.i. $CD4^{-/-}$ mice averaged almost 1-log-higher viral titre (10^5 PFU/gm versus $10^{3.9}$ PFU/gm, *p= 0.016) than $CD4^{+/+}$ mice. On day 15 p.i. there were no detectable viral PFUs in $CD4^{+/+}$ mice, however, a significant number of infectious viral PFUs were observed in $CD4^{-/-}$ mice ($10^{4.6}$ PFU/gm, ****p=0.0001) (Fig. 7a).

To further confirm whether differences in viral replication might affect viral infection, qRT-PCR of viral N-gene (nucleocapsid) from brain tissues from MI, $CD4^{+/+}$, and $CD4^{-/-}$ infected mice was performed. As shown in Fig. 7b, viral persistence is comparable in both $CD4^{+/+}$ and $CD4^{-/-}$ mice (1.02 fold ± 0.176) at day 5 p.i. At day 10 and day 15 p.i., the N-gene transcript shows significant upregulation (10.230 folds ± 2.677, **p= 0.003 and 23.247 folds ± 5.204, ****p< 0.0001, respectively), in $CD4^{-/-}$ mice compared to $CD4^{+/+}$.

To determine the spread of infectious viral particles in situ, immunohistochemical analysis of viral anti-nucleocapsid antigen was performed on sections of infected brains obtained from $CD4^{+/+}$, $CD4^{-/-}$, and MI mice at the acute and chronic phases of infection. In MI mice, viral antigen was neither observed at day 6 nor at day 30 p.i. as expected (Fig. 7c). Post-intra-cranial inoculation, RSA59 replicates profusely in $CD4^{+/+}$ mice and spreads rapidly from the lateral geniculate nuclei to several regions of the brain, including the olfactory bulb, basal forebrain, cerebral cortex, anterior commissure, brain stem and deep cerebellar white matter. By day 6 p.i., viral antigen becomes restricted to the midbrain, pons, and deep cerebellar white matter in the current study (data not shown). Similar viral anti-nucleocapsid antigen staining was observed in infected $CD4^{-/-}$ mice at day 6 p.i. Day 30 post infected brains of $CD4^{+/+}$ mice showed significantly reduced viral antigen staining as expected, whereas a considerable number of cells remained positive for viral anti-nucleocapsid antigen in the $CD4^{-/-}$ mice (Fig. 7c).

Moreover, Interferon gamma (IFN-γ) mRNA expression was significantly higher at day 5 p.i. in $CD4^{-/-}$ mice (2.45 folds ± 0.59, **p=0.0020), Fig. 7d, in comparison to $CD4^{+/+}$ mice,

indicating higher viral replication in $CD4^{-/-}$ mice. Similarly, peripheral leukocyte chemoattractant IFN-γ inducible CXCL10 (a C-X-C chemokine) mRNA expression remained significantly upregulated even at day 10 p.i. (5.102 folds ± 1.253, ***p=0.0008) and day 15 p.i. (2.965 folds ± 0.858,*p=0.015) in the infected $CD4^{-/-}$ mice (Fig. 7e) as compared to $CD4^{+/+}$ mice. Also, anti-viral Tumour Necrosis Factor alpha (TNF-α) mRNA expression was observed to be significantly upregulated at all time points in $CD4^{-/-}$ mice, in comparison to $CD4^{+/+}$ mice (6.372 folds ± 1.10, ****p<0.0001 at day5, 37.949 folds ± 9.534,****p=0.00018 at day 10, and 7.348 folds ± 1.675, ****p<0.0001 at day 15), Fig. 7f. At the same time, $CD4^{-/-}$ mice displayed lower levels of RANTES (Regulated upon Activation, Normal T Cell Expressed and Presumably Secreted) or CCL5 (a C-C chemokine, involved in trafficking of macrophage/monocytes into the CNS) mRNA transcripts at day 5 p.i. (0.523 folds ± 0.124, **p<0.01 and day 10 p.i. (0.544 folds ± 0.214, *p<0.05) in comparison to $CD4^{+/+}$ mice (Fig. 7g)

Viral plaque assays and qRT-PCR of viral N-gene and antiviral-cytokines and chemokines expression (IFN-γ, TNF-α, CXCL10) at day 5, 10 and 15 p.i in corroboration with the viral anti-nucleocapsid antigen staining at day 30 p.i. confirmed prolonged persistence of RSA59 in the absence of functional CD4 in brain tissue.

The absence of $CD4^+$ T cells exacerbates CNS inflammation and myelin loss at the chronic stage of inflammation.

The role of functional $CD4^+$ T cells in demyelination was next examined by histopathological analysis of day 30 post-infected spinal cords from $CD4^{+/+}$ and $CD4^{-/-}$ mice. In $CD4^{+/+}$ mice, inflammation was observed in the dorsal/posterior columns, anterior horn and/or the lateral descending tracts. H&E staining highlights the inflammation in the ventrolateral white matter. In contrast, $CD4^{-/-}$ mice demonstrated vacuolar pathology with swollen axons throughout the white matter, involving the ventral and lateral descending tracts upon H& E staining (Fig. 8a). Corresponding inflamed regions from serial sections also showed myelin loss by LFB staining in both $CD4^{+/+}$ and $CD4^{-/-}$ mice. The degree of demyelination was significantly higher in the $CD4^{-/-}$ mice (20.45 ± 2.174, ****p<0.0001) compared to $CD4^{+/+}$ mice (6.008 ± 1.375) (48) (Fig. 8b). CD45 immunoreactive inflammatory cells were present within the demyelinating plaques in both $CD4^{+/+}$ and $CD4^{-/-}$, however the extent of inflammation was considerably greater in $CD4^{-/-}$ (2.812 ± 0.1122 ,****p<0.0001) mice in comparison to the $CD4^{+/+}$ mice (0.5509 ± 0.08550) (Fig. 8c). Interestingly, in contrast to the acute phase of infection, $CD4^{-/-}$

mice (1.237 ± 0.1646, ***p<0.001) spinal cord showed highly significant CD11b microglia/macrophage expression, in comparison to $CD4^{+/+}$ mice (0.4175 ± 0.09144). (Fig. 8d)

Quite strikingly, in contrast to the brains of $CD4^{+/+}$ (Fig. 9a) mice, $CD4^{-/-}$ mice exhibited extensive vacuolation in the brain stem and the deep cerebellar white matter tracts which has not been observed in previous studies. No significant differences were observed in CD45 staining between the two groups (Fig. 9b). Large numbers of CD11b positive microglia/macrophages were observed in the vicinity of the vacuolated regions in $CD4^{-/-}$ mice (5.251 ± 0.5298, ****p<0.0001) as compared to $CD4^{+/+}$ mice (2.220 ± 0.1639) (Fig. 9c).

The Absence of CD4+ T cells aggravates axonopathy

One-micron thick sections of glutaraldehyde fixed brains and spinal cords from RSA59 infected $CD4^{-/-}$, $CD4^{+/+}$, and MI $CD4^{-/-}$ mice were stained with toluidine blue. MI $CD4^{-/-}$ did not show any visible signs of inflammation (Fig. 10) or spinal cord damage. Infected $CD4^{-/-}$ mice exhibited vacuolation and axonal degeneration in the posterior columns (Fig. 11a, b). Electron microscopy of the vacuolated brainstem lesions in $CD4^{-/-}$ mice revealed that the vacuolation represents numerous swollen degenerating axons, and few inflammatory cells (lymphocytes and macrophages). There was no evidence of isolated demyelination (myelin loss with relative axonal preservation) (data not shown). Similarly, electron micrographs of the spinal cord white matter lesions (Fig. 11c, d) also showed axonal degeneration and a lack of demyelination. No inflammatory cells (lymphocytes and macrophages) were present within the areas of white matter damage (Fig. 11c).

In the absence of $CD4^{+}$ T cells, mice show differential expression of inflammatory cytokines.

The inflammatory cells in the demyelinating lesions induced by RSA59, exhibit variable expression of pro- and anti-inflammatory cytokines. Expression of pro-inflammatory IL-6, IL-12p40, and anti-inflammatory IL-10 were examined in RSA59 infected mouse brains. Quantitative PCR results revealed that IL-6 expression was significantly higher in $CD4^{-/-}$ compared to $CD4^{+/+}$ mice both at day 5 (6.742 folds ± 1.955, ****p<0.0001) and day 10 p.i. (4.24 folds ± 0.912, ****p<0.0001), and subsequently declines at day 15 p.i. in both groups of mice (Fig. 12a). IL-10 expression patterns, as revealed by real-time PCR, showed similar expression in the RSA59 infected $CD4^{+/+}$ and $CD4^{-/-}$ mice at day 5 p.i. However, at days 10 (2.579 folds ± 0.72, **p=0.003) and 15 p.i. (2.58 folds ± 0.363, ****p<0.0001) $CD4^{+/+}$ mice

showed significantly elevated expression of IL-10 compared to infected $CD4^{-/-}$ mice (Fig. 12b). IL-12p40 mRNA expression demonstrated no considerable differences between $CD4^{+/+}$ and $CD4^{-/-}$ mice following RSA59 infection (data not shown). Together the expression patterns of IL-6 and IL-10 indicate a robust inflammatory environment in the brains of $CD4^{-/-}$ mice.

The absence of CD4+ T cells influences macrophage polarization.

Using the classical M1/M2 nomenclature of macrophage polarization, it was observed that mRNA expression of classical M1 macrophage (pro-inflammatory) markers such as CD86 andBruton's tyrosine kinase (Btk) were significantly reduced in infected $CD4^{-/-}$ mice in comparison to $CD4^{+/+}$ mice at day 5 p.i (0.445 folds ± 0.128, ***$p<0.001$ and 0.545 folds ± 0.134, **$p<0.01$, for CD86 and Btk respectively) (Fig. 12c.d). But, as the course of disease progressed toward the chronic phase, microglia/macrophages in the infected $CD4^{-/-}$ mice showed an M2 phenotype (anti-inflammatory) in contrast to the $CD4^{+/+}$ mice, as observed by the significant upregulation in the mRNA expression of M2 macrophage marker CD163 at day 15 p.i. (2.018 folds ± 0.392,****$p<0.0001$) (Fig. 12e).

DISCUSSION

The CNS is no longer considered an immune-privileged site (49). A significant number of peripheral $CD4^+$ T cells patrol the cerebrospinal fluid (CSF) in order to detect the presence of potential harmful pathogens (50-52). If these T cells do not encounter their cognate antigen, they take the lymphatic route to exit the CNS. However, they will infiltrate the CNS parenchyma upon sensing any sign of neuroinflammation (52, 53). MHV infection in mice is an established archetype animal model used to understand the demyelination pathology in MS. In this study, we present a protective role of $CD4^+$ T cells in the viral induced neuroinflammatory demyelination, in contrast to the pathogenic role of $CD4^+$T cells in MS(54) and its autoimmune experimental model EAE. Activated myelinolytic $CD4^+$ T cells have been observed in the blood and cerebrospinal fluid (CSF) of MS patients (7); Additionally, MS lesions have been widely associated with the presence of both $CD4^+$ and $CD8^+$ T cells (55).These autoreactive T cells induce a Th-1 response, majorly targeted against PLP, and can worsen the disease progression in the patients (56-58). Considering their well-acceptedpathogenic role in MS, classical immuno therapies are devised to silence the $CD4^+$ T cell mediated attack on the myelin to repair the damage caused to the myelin sheath. Our study

highlights a quite opposite, protective role of $CD4^+$T cells in a virus induced etiology of demyelination in MS.

In this study, we present evidences to show that spatio-temporal infiltration of $CD4^+$ T cells in the CNS and their dynamic equilibrium with brain resident microglia may influence the progression, severity, and amelioration of white and gray matter inflammation in a neurotropic virus model. The most widely used experimental model of MS, EAE, holds good only for understanding the mechanisms of white matter injury and does not recapitulate the aspects of gray matter damage.

The RSA59-induced demyelinating model is unique, it involves both white and gray matter inflammation. The onset of the disease is initiated via orchestration of innate immune genes in the acute phase to clear the virus and restore homeostasis and then gradually progress via adaptive immunity during the chronic phase (45). RSA59 induced demyelination is dissimilar to other conventional demyelinating models that are explicitly driven by adaptive immune responses, with its array of specialized T cells ($CD4^+$ and $CD8^+$) and myelin antigen-specific antibodies (20, 59, 60). Dynamic host immune responses involving $CD4^+$ helper T cells are needed for recovery from infections. While $CD4^+$ T cells are helpers for the development of a complete adaptive immune response, they are also required for enhancing innate immune effector functions. To assess the role of $CD4^+$ T cells in the innate and adaptive immune responses and their interactions with microglia/macrophages following RSA59 infection, the current study compared $CD4^{-/-}$ mice and wild-type mice. The results showed a critical role of $CD4^+$ T cells in the pathogenesis of RSA59 induced neuroinflammation. We observed the following: i) Absence of $CD4^+$ T cells caused no change in acute encephalitis; but $CD4^{-/-}$ mice showed a significant reduction in CD11b positive microglia/macrophages; ii) viral replication was higher and viral trancripts were persistent in $CD4^{-/-}$ mice, even at day 30 p.i.; iii) $CD4^{-/-}$ mice showed an augmented susceptibility toward chronic phase encephalitis and demyelination. Furthermore, $CD4^{-/-}$ mice, presented with poliomyelitis, bulbar (brainstem) vacuolation of the neuropil, and dorsal root ganglionic inflammation, a finding rarely observed in $CD4^{+/+}$ mice; iv) a strikingly higher number of CD11b positive microglia/macrophages were present in the $CD4^{-/-}$ mice at the chronic infection phase. These microglia/macrophages were disseminated throughout the inflamed regions of white matter and in the areas of gray matter, both in the brain and spinal cord at the chronic infection phase; and v) Electron microscopy revealed axonal degeneration in the spinal cords of $CD4^{-/-}$ mice even in the absence of

inflammation, suggesting that white matter degeneration occurs secondary to neuronal injury without a direct attack of inflammatory cells upon spinal cord myelin sheaths.

Our results also revealed substantially higher mRNA expression levels of IFNγ, TNFα, and IFN inducible leukocyte chemoattractant CXCL10 in the $CD4^{-/-}$ mice in comparison to $CD4^{+/+}$ mice which is likely a response to recruit further peripheral lymphocytes into the CNS to combat the persistent viral load in the former. The increased and uncontrolled viral replication contributes to severe inflammation and neuronal cell body damage observed in the gray matter of the spinal cord and dorsal root ganglion of the $CD4^{-/-}$ mice. Elevated mRNA levels of pro-inflammatory cytokine IL-6 at day 5 and 10 p.i. along with persistent viral load signifies a robust pro-inflammatory environment in the CNS of $CD4^{-/-}$ mice. Expression of the anti-inflammatory cytokine IL-10 remains almost constant throughout the study in $CD4^{+/+}$ mice, while its expression in $CD4^{-/-}$ is consistently low, suggesting that $CD4^{+}$ T cells serve as one of the key sources of IL-10 production.

Apart from this, it was interesting to note that anti-viral chemokine CCL5 or RANTES (macrophage/monocyte chemoattractant) was downregulated in $CD4^{-/-}$ mice at day 5 and 10 p.i., perhaps as a result of which a significant reduction in CD11b positive inflammatory cells was observed in the brains and spinal cords at the acute phase of inflammation. Nevertheless, overall encephalitis at the acute phase, as shown by CD45 staining, was comparable in both $CD4^{+/+}$ and $CD4^{-/-}$ mice, suggesting that the initial inflammation in the CNS is independent of CD4++ T cells. This finding also hints that the fewer numbers of CD11b+ cells might be the result of dampened infiltration of monocyte/macrophages in the absence of functional $CD4^{+}$ T cells and the CD11b+ cells observed in the CNS might correspond to the brain resident microglia.

The function and role of microglia as mediators of homeostasis in the CNS is well established (61). They not only act as custodians of CNS immunity but also protect neurons during development and monitor synaptogenesis (62). However, during pathological conditions, microglia attain a signature pro-inflammatory state that is directed toward the clearance of toxic substances from the CNS (63, 64). M1 or classically activated microglia can also induce the activation of A1 astrocytes, which develop altered ability to promote neuroprotection (65). A2 astrocytes are activated by M2 microglia (alternatively activated) and help in CNS repair and protection (66). Examination of mRNA expression revealed a higher expression of pro-inflammatory M1 markers CD86 and Btk in the CNS of $CD4^{+/+}$ mice during the acute infection.

CD163 mRNA transcripts increased in expression in the $CD4^{+/+}$ mice during day 10 p.i. and then declined with the restoration of homeostasis, but $CD4^{-/-}$ mice showed a significant increase in the expression of CD163 mRNA even at day 15 p.i. suggesting that the CD11b+ microglia/macrophages present during the transition phase (from acute to chronic) in the CNS might be of the M2 phenotype (anti-inflammatory) attempting to combat the prolonged viral persistence and restore homeostasis to prevent further tissue damage, but fail to do so without the help of $CD4^{+}$T cells. Though M2 microglia/macrophages are categorized as anti-inflammatory, they are also reported to have high phagocytic ability. Their activation and persistence might, therefore, promote direct myelin stripping as previously reported (40) leading to significantly greater demyelination and axonal loss in the $CD4^{-/-}$ mice.

An interesting question that remains to be answered is if the infiltration of monocyte/macrophages is impeded in the first place, why is there a higher expression of CD11b positive cells in the CNS of $CD4^{-/-}$ mice during the chronic phase? To answer this, future experiments are aimed at performing immunophenotyping of the inflammatory cells, using flow cytometry in the $CD4^{-/-}$ mice, to explicitly decipher whether the cells present at the chronic phase are predominately peripherally recruited monocytes/macrophages or the activated resident phagocytic microglial cells of the CNS. So far, flow cytometric analysis in $CD4^{+/+}$ mice has shown the presence of a significant population of CD11b hi/ CD45 lo (microglia) at day 30 p.i. but very little or no CD11b expressing CD45 high monocyte/macrophages in the CNS (data not shown). We, therefore, expect the CD11b+ cells found in the CNS at day 30 in the $CD4^{-/-}$ mice to be microglia and not peripherally recruited myeloid cells.

For this study, we have opted for a mouse strain (B6.129S2-$Cd4^{tm1Mak}$/J) where the functionality of $CD4^{+}$ T helper cells was disrupted. The development of $CD8^{+}$ T cell and myeloid components was unaffected. 90% of the circulating T cells were CD8+ and their cytotoxic activity was within normal ranges (67). Despite the presence of functional $CD8^{+}$ T cells, viral clearance was substantially delayed. Thus, our studies suggest a vast preponderance of $CD4^{+}$ T cells over $CD8^{+}$ T cells in maintaining the homeostasis upon RSA59 induced neuroinflammation.

In conclusion, our results demonstrate that $CD4^{+}$ T cells are necessary for eliminating viral particles, promoting microglial polarization toward anti-inflammation, and controlling chronic progressive axonal degeneration. The current study also highlights the importance of $CD4^{+}$T cells beyond the classic inflammatory lesions of the white matter tract. We have shown that

gray matter inflammation in the form of poliomyelitis is significantly exacerbated in the absence of $CD4^+$ T cells. Moreover, we show that the imprinting of the microglia/macrophage-mediated inflammatory innate immune response on the consequent protective adaptive immunity requires functional $CD4^+$ T cells. This communication between microglia and T cells is a highly regulated, interdependent, and bidirectional process and is critical for the establishment of an effective immune response. Although innate anti-viral immune responses by microglia are crucial in controlling the initial CNS viral dissemination, virus-specific T cells are essential to eliminate the virus and provide indispensable neuroprotection. Further studies will be conducted to understand the nexus between CNS resident microglia/monocyte-derived macrophages with infiltrating activated T helper cells at the molecular level through immune-coregulatory CD40-CD40 ligand (L) pathway. This dyad is broadly recognized for its essential role in immune regulation and homeostasis. Our studies will be focused to examine such interactions at the molecular level using CD40 and CD40L deficient mice in the outcome of inflammatory demyelinationMost MS therapies are aimed at preventing damage to myelin by regulating the multiple components of adaptive immune system,especially the T cell subsets (Th1, Th2, Th17, $CD8^+$, NKT, $CD4^+CD25^+$ T regulatory cells) and B cells. Current therapies have only been able to reduce the number and rate of MS lesion formation and are only partially efficacious(68). Understanding the role of T cells in a viral induced model of MS is thus critical to design more robust therapeutics. Together these studies can help to expand our knowledge intended to use CD4 mediated immune therapy as a potential treatment of MS, depending on its etiologyand the initiation of the pathology.

MATERIALS AND METHODS

Virus, Inoculation of mice and Experimental design

Recombinant isogenic demyelinating (DM) strain of MHV-A59, RSA59, was used to infect mice as formerly described (39). Four to five-week old, MHV-free, $CD4^{+/+/+/+}$ C57BL/6 (B6) mice (Jackson Laboratory) and $CD4^{-/-}$ (B6.129S2-$Cd4^{tm1Mak}$/J) mice (Jackson Laboratory, Stock no. 002663) were used for the study. The $CD4^{-/-}$ mice obtained from Jackson's laboratory is homozygous for the $Cd4^{tm1Mak}$ targeted mutation, have a significant blockade in the $CD4^+$ T-cell development and show an MHC class II restricted T helper cell activity(67). The mice were inoculated intracranially with 25,000 (50% of LD50) PFU of RSA59 strain as described previously. Likewise, mock-infected controls for $CD4^{+/+}$ and $CD4^{-/--/-}$ mice were inoculated with an uninfected cell lysate (PBS+0.075% BSA) at an equivalent dilution. Mice were

monitored daily post infection (p.i.) for disease signs and symptoms. Clinical disease severity was graded using the following scale: 0, no disease symptoms; 1, ruffled fur; 1.5, hunched back with mild ataxia: 2, Ataxia, balance problem and hind limb weakness: 2.5 one leg completely paralyzed, motility issue but still able to move around with difficulties; 3, severe hunching/wasting/both hind limb paralysis and mobility is severely compromised;3.5 Severe distress, complete paralysis and moribund 4, dead (47).

For EM, histopathological, and immunohistochemical analyses mice were sacrificed at the acute infection phase, i.e. on day 5-6 (four mice per group), and chronic infection phase, i.e. day 30 (five mice per group) post-infection. For RNA and protein studies and viral titer estimation, animals were sacrificed (3 mice per group) on days 5, 10 and 15 post-infection.

Estimation of Viral Replication

Mice were euthanized on days 5, 10 and 15 post-infection and perfused transcardially with 20 ml of sterile PBS. Brains were harvested for determination of viral titers and placed into 1 ml of isotonic saline containing 0.167% gelatin (gel saline). Brain tissues were weighed and kept frozen at -80°C until titred. Tissues were subsequently homogenized, and viral titers were quantified by standard plaque assay protocol on tight monolayers of L2 cells as described previously with minor modifications (39).

Histopathology and Immunohistochemical Analysis

Mice were sacrificed at day 6 and day 30 post-infection. Following transcardial perfusion with PBS and 4% paraformaldehyde, liver, brain, and spinal cord tissues were harvested and embedded in paraffin. Five-micron thick sections of the embedded tissues were prepared and stained with Hematoxylin and Eosin for histopathologic analysis. Luxol fast blue (LFB) staining was performed to evaluate demyelination in the brain and spinal cord tissues, as described previously with minor modifications (40).

Immunohistochemical staining of brain and spinal cord tissue sections used the following primary antibodies - 1:10000 dilution of anti-CD11b (Abcam, Cat #:ab133357), 1:200 dilution of anti-CD45 (LCA; leukocyte common antigen, BD Pharmingen Cat#:550539) and 1:40 dilution of monoclonal antibody directed against the nucleocapsid protein (N) of MHV (monoclonal antibody clone 1-16-1 provided by Julian Leibowitz, Texas A&M University). Bound primary antibodies were detected by an avidin-biotin immunoperoxidase technique

(Vector Laboratories) using 3, 3-diaminobenzidine as the substrate. Control slides from mock-infected mice were stained in parallel. All slides were coded and read in a blinded manner by the same investigator, as described previously with minor modifications (40).

H&E Sections were assessed for inflammation in the following manner: 0, none; 1, few inflammatory cells; 2, organization of perivascular infiltrates; and 3, increasing severity of perivascular cuffing and formation of microglial nodules, and represented in Table 1 (47).

Quantification of histopathological sections

The number of hepatic lesions were counted per section and averaged for each mouse at each time point (both acute and chronic phase of inflammation). The functional scoring of the inflammatory lesions in the liver was characterized as the Hepatic activity index (HAI). Degree of activity was categorized as portal inflammation; Interphase hepatitis (Piecemeal necrosis); Focal (Spotty) necrosis, apoptosis, and focal inflammation; and Confluent necrosis. Scores from 0-6 were allotted for each category based on the modified Knodell's HAI, commonly referred to as the Ishak system (69).

Image analysis was performed using the basic densitometric thresholding application of Fiji (Image J, NIH Image, Scion Image) as described previously (48). Briefly, image analysis for CD45 and CD11b stained sections was performed by capturing the images at the highest magnification (4X-for brain, 10X-for spinal cord) such that the entire section (i.e., scan area) can be visualized within a single frame. The RGB image was deconvoluted into three different colours to separate and subtract the DAB-specific staining from the background H&E staining. The perimeter of each brain and spinal cord tissue was digitally outlined, and the area was calculated in μm^2. A threshold value was fixed for each image to make sure that all antibody marked cells are taken into consideration. The amount of CD45, and CD11b staining was termed as the '% area of staining'.

To determine the area of demyelination, LFB-stained spinal cord cross-sections from each mouse were chosen and analyzed using Fiji software (Image J 1.52g). The total perimeter of the white matter regions in each cross-section was marked and calculated by adding together the dorsal, ventral and anterior white matter areas in each section. Also, the total area of the demyelinated regions was outlined and collated for each section separately. The percentage of spinal cord demyelination per section per mouse was calculated.

Gene Expression: RNA Isolation, Reverse transcription and quantitative Polymerase chain reaction

RNA was extracted from brain tissues (flash-frozen) of RSA59 infected $CD4^{+/+}$ and $CD4^{-/-}$ and mock-infected mice (3 from each group at days 5, 10 and 15 p.i.) using the Trizol isolation protocol following transcardial perfusion with DEPC treated PBS. The total RNA concentration was measured using a NanoDrop ND-100 spectrophotometer. 1µg of RNA was used to prepare cDNA using a High Capacity cDNA Reverse Transcription Kit (Applied Biosystems). Quantitative Real-time PCR analysis was performed using DyNAmo Color Flash SYBR Green qPCR kit (Thermo Scientific) in a Step One plus Real-time PCR system (Thermo Fisher Scientific) under the following conditions: initial denaturation at 95°C for 7 min, 40 cycles of 95°C for 10 s, 60°C for 30 s, melting curve analysis at 60°C for 30 s. Reactions were performed in triplicate. Sequences for the primers used are given in Table III. Relative quantitation was achieved using the comparative threshold (ΔΔCt) method. mRNA expression levels of target genes in RSA59 infected $CD4^{+/+}$ and $CD4^{-/-}$ mice were normalized with β-Actin and expressed as relative fold change compared to their respective mock-infected controls.

Ultra-structural studies and electron microscopy to characterize the preservation of myelin and axons

To characterize axonal blebbing, disruption of the myelin sheath, and axon-myelin coherence, ultrastructural studies were carried out on the brains, brainstem and spinal cords of mice. Infected $CD4^{-/-}$, $CD4^{+/+}$ and $CD4^{-/-}$ mock-infected mice were anesthetized and sacrificed at day 28 p.i. Mice were perfused with 4% PFA. Brains and spinal cords were harvested and fixed overnight in 2% glutaraldehyde, post-fixed with 1% osmium tetroxide, and dehydrated in a graded series of ethanol washes. For transmission electron microscopy, samples were flat embedded in Poly-Bed 812 epoxy resin (Polysciences) and sectioned (500 nm) from the lesional epicenter. Toluidine blue staining was performed for examination by light microscopy. Ultrathin TEM sections (600 Å) were trimmed from the representative foci of interest from toluidine blue-stained sections and mounted on 200 mesh copper grids, stained with uranyl acetate and bismuth subnitrite, and viewed under a JEOL JEM 1010 electron microscope (40).

Statistical Analyses

The viral titer was calculated as plaque-forming units (PFU) based on the following formula = (no. of plaques X dilution factor/ml/gram of tissue). Virus titer was expressed as $\log_{10}$

PFU/gram of tissue. Quantitative RT-PCR data were presented as mean values ± SEM. Values were subjected to Two-Way ANOVA/Student's t-test analysis for calculating the significance of differences between the means. Also, multiple comparisons were achieved by the Tukey test and the Holm-Sidak test. All statistical analyses were done using GraphPad Prism 6 (La Jolla, CA). A P-value of <0.05 was considered statistically significant.

ACKNOWLEDGEMENTS

This work was supported by the Department of Biotechnology [BT/PR 20922/MED/122/37/2016] research grant, India; Animal facility, University of Pennsylvania; Histopathology core, Thomas Jefferson University, Philadelphia, USA; NIH grant EY015014; Research to Prevent Blindness; and the F. M. Kirby Foundation. We thank IISER-Kolkata animal facility for providing necessary support. We thank Ministry of Human Resource Development (MHRD), India, Council of Scientific and Industrial Research (CSIR), India and University Grants Comission (UGC), India for fellowships to DC, FS, AB and SK.

DECLARATIONS

Ethics approval

All experimental procedures and animal care and use were strictly regulated and reviewed in accordance with good animal ethics approved by the Institutional Animal Care and Use Committee at the Indian Institute of Science Education and Research Kolkata (AUP No. IISERK/IAEC/AP/2017/15) and the University of Pennsylvania, Philadelphia, USA (IACUC Protocol No. 804701). Experiments were performed following the guidelines of the Committee for the Purpose of Control and Supervision of Experiments on Animals (CPCSEA) , India and the United States National Institutes of Health Office of Laboratory Animal Welfare Guide for the Care and Use of Laboratory Animals, 8th Edition.

Consent for publication

Not Applicable

Availability of data and materials

The datasets used and/or analyzed during the current study will be made available from the corresponding author on reasonable request.

Author Contribution

DC, FD and JDS designed and planned all the experiments. DC, and FS performed the experiments. DC, FS, and JDS analyzed the data and wrote the manuscript. AB, SK, RK and KD helped with the standardization of RNA experiments in the knockout mice. LK blindly read the pathological samples. JDS, KS and LK participated in data analysis and data interpretation. LK and KS were involved in critical revisions of the manuscript. JDS and KS jointly supervised and reviewed this work.

Competing interests

The authors declare that they have no competing interests.

REFERENCES

1. Glass CK, Saijo K, Winner B, Marchetto MC, Gage FH. 2010. Mechanisms Underlying Inflammation in Neurodegeneration. Cell 140:918-934.
2. Waisman A, Liblau RS, Becher B. 2015. Innate and adaptive immune responses in the CNS. The Lancet Neurology 14:945-955.
3. Prinz M, Priller J. 2017. The role of peripheral immune cells in the CNS in steady state and disease. Nature Neuroscience 20:136-144.
4. Schetters STT, Gomez-Nicola D, Garcia-Vallejo JJ, Van Kooyk Y. 2018. Neuroinflammation: Microglia and T Cells Get Ready to Tango. Frontiers in immunology 8:1905-1905.
5. McFarlin DE, McFarland HF. 1982. Multiple sclerosis (second of two parts). The New England journal of medicine 307:1246-1251.
6. McFarlin DE, McFarland HF. 1982. Multiple sclerosis (first of two parts). The New England journal of medicine 307:1183-1188.
7. Zhang J, Markovic-Plese S, Lacet B, Raus J, Weiner HL, Hafler DA. 1994. Increased frequency of interleukin 2-responsive T cells specific for myelin basic protein and proteolipid protein in peripheral blood and cerebrospinal fluid of patients with multiple sclerosis. The Journal of experimental medicine 179:973-984.
8. Martin R, McFarland HF. 1995. Immunological aspects of experimental allergic encephalomyelitis and multiple sclerosis. Critical reviews in clinical laboratory sciences 32:121-182.
9. Steinman L. 1996. Multiple sclerosis: a coordinated immunological attack against myelin in the central nervous system. Cell 85:299-302.
10. Sospedra M, Martin R. 2005. Immunology of multiple sclerosis. Annual review of immunology 23:683-747.
11. Kuchroo VK, Anderson AC, Waldner H, Munder M, Bettelli E, Nicholson LB. 2002. T cell response in experimental autoimmune encephalomyelitis (EAE): role of self and cross-reactive antigens in shaping, tuning, and regulating the autopathogenic T cell repertoire. Annual review of immunology 20:101-123.
12. Langrish CL, Chen Y, Blumenschein WM, Mattson J, Basham B, Sedgwick JD, McClanahan T, Kastelein RA, Cua DJ. 2005. IL-23 drives a pathogenic T cell population that induces autoimmune inflammation. The Journal of experimental medicine 201:233-240.

13. Martin B, Hirota K, Cua DJ, Stockinger B, Veldhoen M. 2009. Interleukin-17-producing gammadelta T cells selectively expand in response to pathogen products and environmental signals. Immunity 31:321-330.
14. Reboldi A, Coisne C, Baumjohann D, Benvenuto F, Bottinelli D, Lira S, Uccelli A, Lanzavecchia A, Engelhardt B, Sallusto F. 2009. C-C chemokine receptor 6-regulated entry of TH-17 cells into the CNS through the choroid plexus is required for the initiation of EAE. Nature immunology 10:514-523.
15. Das Sarma J, Ciric B, Marek R, Sadhukhan S, Caruso ML, Shafagh J, Fitzgerald DC, Shindler KS, Rostami A. 2009. Functional interleukin-17 receptor A is expressed in central nervous system glia and upregulated in experimental autoimmune encephalomyelitis. Journal of neuroinflammation 6:14-14.
16. Murphy ÁC, Lalor SJ, Lynch MA, Mills KHG. 2010. Infiltration of Th1 and Th17 cells and activation of microglia in the CNS during the course of experimental autoimmune encephalomyelitis. Brain, Behavior, and Immunity 24:641-651.
17. Li J, Zhao X, Hao H-W, Shaw MK, Tse HY. 2011. T cells that trigger acute experimental autoimmune encephalomyelitis also mediate subsequent disease relapses and predominantly produce IL-17. Journal of neuroimmunology 230:26-32.
18. Rostami A, Ciric B. 2013. Role of Th17 cells in the pathogenesis of CNS inflammatory demyelination. Journal of the neurological sciences 333:76-87.
19. Hirota K, Duarte JH, Veldhoen M, Hornsby E, Li Y, Cua DJ, Ahlfors H, Wilhelm C, Tolaini M, Menzel U, Garefalaki A, Potocnik AJ, Stockinger B. 2011. Fate mapping of IL-17-producing T cells in inflammatory responses. Nature immunology 12:255-263.
20. Huseby ES, Liggitt D, Brabb T, Schnabel B, Ohlén C, Goverman J. 2001. A pathogenic role for myelin-specific CD8(+) T cells in a model for multiple sclerosis. The Journal of experimental medicine 194:669-676.
21. Sun D, Whitaker JN, Huang Z, Liu D, Coleclough C, Wekerle H, Raine CS. 2001. Myelin antigen-specific CD8+ T cells are encephalitogenic and produce severe disease in C57BL/6 mice. Journal of immunology (Baltimore, Md : 1950) 166:7579-7587.
22. Wagner CA, Roqué PJ, Mileur TR, Liggitt D, Goverman JM. 2020. Myelin-specific CD8+ T cells exacerbate brain inflammation in CNS autoimmunity. The Journal of clinical investigation 130:203-213.
23. Lane TE, Liu MT, Chen BP, Asensio VC, Samawi RM, Paoletti AD, Campbell IL, Kunkel SL, Fox HS, Buchmeier MJ. 2000. A central role for CD4(+) T cells and RANTES in virus-induced central nervous system inflammation and demyelination. Journal of virology 74:1415-1424.
24. Wu GF, Dandekar AA, Pewe L, Perlman S. 2000. CD4 and CD8 T cells have redundant but not identical roles in virus-induced demyelination. Journal of immunology (Baltimore, Md : 1950) 165:2278-2286.
25. Gagliano SA, Pouget JG, Hardy J, Knight J, Barnes MR, Ryten M, Weale ME. 2016. Genomics implicates adaptive and innate immunity in Alzheimer's and Parkinson's diseases. Annals of clinical and translational neurology 3:924-933.
26. González H, Pacheco R. 2014. T-cell-mediated regulation of neuroinflammation involved in neurodegenerative diseases. Journal of neuroinflammation 11:201-201.
27. Browne TC, McQuillan K, McManus RM, O'Reilly J-A, Mills KHG, Lynch MA. 2013. IFN-γ Production by amyloid β-specific Th1 cells promotes microglial activation and increases plaque burden in a mouse model of Alzheimer's disease. Journal of immunology (Baltimore, Md : 1950) 190:2241-2251.
28. Zhang J, Ke K-F, Liu Z, Qiu Y-H, Peng Y-P. 2013. Th17 cell-mediated neuroinflammation is involved in neurodegeneration of aβ1-42-induced Alzheimer's disease model rats. PloS one 8:e75786-e75786.
29. Saresella M, Piancone F, Tortorella P, Marventano I, Gatti A, Caputo D, Lunetta C, Corbo M, Rovaris M, Clerici M. 2013. T helper-17 activation dominates the immunologic milieu of both

amyotrophic lateral sclerosis and progressive multiple sclerosis. Clinical immunology (Orlando, Fla) 148:79-88.
30. Brochard V, Combadière B, Prigent A, Laouar Y, Perrin A, Beray-Berthat V, Bonduelle O, Alvarez-Fischer D, Callebert J, Launay J-M, Duyckaerts C, Flavell RA, Hirsch EC, Hunot S. 2009. Infiltration of CD4+ lymphocytes into the brain contributes to neurodegeneration in a mouse model of Parkinson disease. The Journal of clinical investigation 119:182-192.
31. Beers DR, Henkel JS, Zhao W, Wang J, Appel SH. 2008. CD4+ T cells support glial neuroprotection, slow disease progression, and modify glial morphology in an animal model of inherited ALS. Proceedings of the National Academy of Sciences of the United States of America 105:15558-15563.
32. Zheng C, Zhou X-W, Wang J-Z. 2016. The dual roles of cytokines in Alzheimer's disease: update on interleukins, TNF-α, TGF-β and IFN-γ. Translational neurodegeneration 5:7-7.
33. Stohlman SA, Hinton DR, Parra B, Atkinson R, Bergmann CC. 2008. CD4 T Cells Contribute to Virus Control and Pathology following Central Nervous System Infection with Neurotropic Mouse Hepatitis Virus. 82:2130-2139.
34. Murray PD, Pavelko KD, Leibowitz J, Lin X, Rodriguez M. 1998. CD4(+) and CD8(+) T cells make discrete contributions to demyelination and neurologic disease in a viral model of multiple sclerosis. Journal of Virology 72:7320-7329.
35. Togo T, Akiyama H, Iseki E, Kondo H, Ikeda K, Kato M, Oda T, Tsuchiya K, Kosaka K. 2002. Occurrence of T cells in the brain of Alzheimer's disease and other neurological diseases. Journal of neuroimmunology 124:83-92.
36. Strachan-Whaley M, Rivest S, Yong VW. 2014. Interactions between microglia and T cells in multiple sclerosis pathobiology. Journal of interferon & cytokine research : the official journal of the International Society for Interferon and Cytokine Research 34:615-622.
37. Garber C, Soung A, Vollmer LL, Kanmogne M, Last A, Brown J, Klein RS. 2019. T cells promote microglia-mediated synaptic elimination and cognitive dysfunction during recovery from neuropathogenic flaviviruses. Nature Neuroscience 22:1276-1288.
38. Lavi E, Gilden DH, Wroblewska Z, Rorke LB, Weiss SR. 1984. Experimental demyelination produced by the A59 strain of mouse hepatitis virus. Neurology 34:597-603.
39. Das Sarma J, Scheen E, Seo S-h, Koval M, Weiss SR. 2002. Enhanced green fluorescent protein expression may be used to monitor murine coronavirus spread in vitro and in the mouse central nervous system. Journal of NeuroVirology 8:381-391.
40. Das Sarma J, Kenyon LC, Hingley ST, Shindler KS. 2009. Mechanisms of Primary Axonal Damage in a Viral Model of Multiple Sclerosis. The Journal of Neuroscience 29:10272-10280.
41. Stohlman SA, Weiner LP. 1981. Chronic central nervous system demyelination in mice after JHM virus infection. Neurology 31:38-44.
42. Sutherland RM, Chua MM, Lavi E, Weiss SR, Paterson Y. 1997. CD4+ and CD8+ T cells are not major effectors of mouse hepatitis virus A59-induced demyelinating disease. Journal of neurovirology 3:225-228.
43. Shindler KS, Kenyon LC, Dutt M, Hingley ST, Das Sarma J. 2008. Experimental optic neuritis induced by a demyelinating strain of mouse hepatitis virus. Journal of virology 82:8882-8886.
44. Houtman JJ, Fleming JO. 1996. Pathogenesis of mouse hepatitis virus-induced demyelination. Journal of neurovirology 2:361-376.
45. Biswas K, Chatterjee D, Addya S, Khan RS, Kenyon LC, Choe A, Cohrs RJ, Shindler KS, Das Sarma J. 2016. Demyelinating strain of mouse hepatitis virus infection bridging innate and adaptive immune response in the induction of demyelination. Clinical immunology (Orlando, Fla) 170:9-19.
46. Chatterjee D, Addya S, Khan RS, Kenyon LC, Choe A, Cohrs RJ, Shindler KS, Sarma JD. 2014. Mouse hepatitis virus infection upregulates genes involved in innate immune responses. PloS one 9:e111351-e111351.

47. Kishore A, Kanaujia A, Nag S, Rostami AM, Kenyon LC, Shindler KS, Das Sarma J. 2013. Different mechanisms of inflammation induced in virus and autoimmune-mediated models of multiple sclerosis in C57BL6 mice. BioMed research international 2013:589048-589048.
48. Singh M, Kishore A, Maity D, Sunanda P, Krishnarjuna B, Vappala S, Raghothama S, Kenyon LC, Pal D, Das Sarma J. 2019. A proline insertion-deletion in the spike glycoprotein fusion peptide of mouse hepatitis virus strongly alters neuropathology. doi:10.1074/jbc.RA118.004418.
49. Zipp F, Aktas O. 2006. The brain as a target of inflammation: common pathways link inflammatory and neurodegenerative diseases. Trends in neurosciences 29:518-527.
50. Aspelund A, Antila S, Proulx ST, Karlsen TV, Karaman S, Detmar M, Wiig H, Alitalo K. 2015. A dural lymphatic vascular system that drains brain interstitial fluid and macromolecules. The Journal of experimental medicine 212:991-999.
51. Engelhardt B, Ransohoff RM. 2005. The ins and outs of T-lymphocyte trafficking to the CNS: anatomical sites and molecular mechanisms. Trends in immunology 26:485-495.
52. Louveau A, Smirnov I, Keyes TJ, Eccles JD, Rouhani SJ, Peske JD, Derecki NC, Castle D, Mandell JW, Lee KS, Harris TH, Kipnis J. 2015. Structural and functional features of central nervous system lymphatic vessels. Nature 523:337-341.
53. Kivisäkk P, Mahad DJ, Callahan MK, Trebst C, Tucky B, Wei T, Wu L, Baekkevold ES, Lassmann H, Staugaitis SM, Campbell JJ, Ransohoff RM. 2003. Human cerebrospinal fluid central memory CD4+ T cells: evidence for trafficking through choroid plexus and meninges via P-selectin. Proceedings of the National Academy of Sciences of the United States of America 100:8389-8394.
54. Zhang J, Weiner HL, Hafler DA. 1992. Autoreactive T Cells in Multiple Sclerosis. International Reviews of Immunology 9:183-201.
55. Raine CS. 1994. The Dale E. McFarlin memorial lecture: The immunology of the multiple sclerosis lesion. Annals of Neurology 36:S61-S72.
56. Kaushansky N, Zhong M-C, Kerlero de Rosbo N, Hoeftberger R, Lassmann H, Ben-Nun A. 2006. Epitope Specificity of Autoreactive T and B Cells Associated with Experimental Autoimmune Encephalomyelitis and Optic Neuritis Induced by Oligodendrocyte-Specific Protein in SJL/J Mice. The Journal of Immunology 177:7364.
57. Kaushansky N, Altmann DM, David CS, Lassmann H, Ben-Nun A. 2012. DQB1*0602 rather than DRB1*1501 confers susceptibility to multiple sclerosis-like disease induced by proteolipid protein (PLP). Journal of Neuroinflammation 9:29.
58. Panitch H, Haley A, Hirsch R, Johnson K. 1987. Exacerbations of Multiple Sclerosis in patients treated with gamma Interferon. The Lancet 329:893-895.
59. Bernard CC. 1976. Experimental autoimmune encephalomyelitis in mice: genetic control of susceptibility. J Immunogenet 3:263-74.
60. Miller SD, Vanderlugt CL, Begolka WS, Pao W, Yauch RL, Neville KL, Katz-Levy Y, Carrizosa A, Kim BS. 1997. Persistent infection with Theiler's virus leads to CNS autoimmunity via epitope spreading. Nat Med 3:1133-6.
61. Shemer A, Erny D, Jung S, Prinz M. 2015. Microglia Plasticity During Health and Disease: An Immunological Perspective. Trends in Immunology 36:614-624.
62. Squarzoni P, Thion M, Garel S. 2015. Neuronal and microglial regulators of cortical wiring: usual and novel guideposts. Frontiers in Neuroscience 9.
63. Prinz M, Priller J. 2014. Microglia and brain macrophages in the molecular age: from origin to neuropsychiatric disease. Nature Reviews Neuroscience 15:300.
64. Biber K, Möller T, Boddeke E, Prinz M. 2015. Central nervous system myeloid cells as drug targets: current status and translational challenges. Nature Reviews Drug Discovery 15:110.
65. Liddelow SA, Guttenplan KA, Clarke LE, Bennett FC, Bohlen CJ, Schirmer L, Bennett ML, Münch AE, Chung W-S, Peterson TC, Wilton DK, Frouin A, Napier BA, Panicker N, Kumar M, Buckwalter MS, Rowitch DH, Dawson VL, Dawson TM, Stevens B, Barres BA. 2017. Neurotoxic reactive astrocytes are induced by activated microglia. Nature 541:481.

66. Anderson MA, Burda JE, Ren Y, Ao Y, O'Shea TM, Kawaguchi R, Coppola G, Khakh BS, Deming TJ, Sofroniew MV. 2016. Astrocyte scar formation aids CNS axon regeneration. Nature 532:195-200.
67. Rahemtulla A, Fung-Leung WP, Schilham MW, Kündig TM, Sambhara SR, Narendran A, Arabian A, Wakeham A, Paige CJ, Zinkernagel RM, Miller RG, Mak TM. 1991. Normal development and function of CD8+ cells but markedly decreased helper cell activity in mice lacking CD4. Nature 353:180-184.
68. Podbielska M, Banik NL, Kurowska E, Hogan EL. 2013. Myelin recovery in multiple sclerosis: the challenge of remyelination. Brain sciences 3:1282-1324.
69. Goodman ZD. 2007. Grading and staging systems for inflammation and fibrosis in chronic liver diseases. Journal of hepatology 47:598-607.

FIGURE LEGENDS

Fig. 1. Temporal immune cell kinetics in the brains of RSA59 infected mice. Results from flow cytometric analysis of the migration of inflammatory cells and CNS resident cells from the RSA59 infected mice has been summarized in the schematic diagram. The diagram represents the differential infiltration of total myeloid (neutrophils, macrophage/monocytes and microglia) and lymphoid (CD4, CD8 and NKT) cell populations during days 3, 5, 7, 10, 16 and 30 p.i. Respective peaks show highest infiltration at times post infection. ScaleArbitrary.

Fig. 2. Absence of CD4 causes no significant pathology in the mock infected mice. $CD4^{+/+}$ and $CD4^{-/-}$ mice were infected with with an uninfected cell lysate (PBS+0.075% BSA). 5-micron thick liver,brain and spinal cord sections were stained with H&E and CD45 for routine histopathological studies. No inflammation was observed in $CD4^{+/+}$ and $CD4^{-/-}$ mice tissues. Data are represented from 3 independent biological replicates. Scale bars= 50 microns

Fig.3 Absence of CD4 shows no significant alterations in RSA59 induced Liver pathology. $CD4^{+/+}$ and $CD4^{-/-}$ mice were infected with RSA59 and 5-micron thick liver sections were stained with H&E for routine morphological studies. a) Both $CD4^{+/+}$ and $CD4^{-/-}$ mice showed similar features of necrotic/non-necrotic hepatitis. Hepatic Activity Index was calculated according to Ishak's Score as described in materials and methods and plotted (b). c) The average number of hepatic lesions were counted per section from each mouse, combined results were tabulated. Liver sizes and cross-sectional areas were comparable in both $CD4^{+/+}$ and $CD^{-/-}$ mice. Data are represented from 5 independent biological experiments.

Fig.4 Absence of CD4 demonstrates no significant changes in encephalomyelitis upon RSA59 induced acute infection. a, b) At day 6 p.i., sections of brain (panel a) and spinal cord

(panel b) from $CD4^{+/+}$ mice and $CD4^{-/-}$ mice were stained with H&E and immunohistochemically for LCA (leucocyte common antigen). Boxed areas are shown at higher magnification below the corresponding brain midsagittal sections (panel a) or cross sections of spinal cord (panel b). The arrows in the zoomed sections mark characteristic perivascular cuffing and microglial nodule formation mediated by infiltrating inflammatory cells in the H&E-stained sections which correspond to immunoreactive leukocytes and microglia/macrophages in the CD45 immunohistochemically stained sections. Scale bars of midsagittal brain sections represent 1000 microns whereas they represent 100 microns in the higher magnification images shown below. Scale bars of spinal cord cross sections represent 200 microns whereas they represent 50 microns in the higher magnification images shown below. Quantification of the intensity of staining is plotted in a scatter diagram. Statistical analysis was performed using Student's t-test and Welch correction. Data are represented from 5 independent biological experiments.

Fig.5 Absence of CD4 resulted in a significant reduction of CD11b positive microglia/macrophages in the brain and spinal cords during RSA59 induced acute infection. At day 6 p.i., sections of brain and spinal cord from $CD4^{+/+}$ mice and $CD4^{-/-}$ mice were immunohistochemically stained for CD11b (macrophage/microglia activation marker). Boxed areas are shown at higher magnification below the corresponding brain midsagittal sections (upper panel) or cross sections of spinal cord (lower panel). Arrows mark microglia/macrophages in the in the CD11b immunohistochemcally stained sections. Scale bars of midsagittal brain sections represent 500 microns whereas they represent 200 microns in the higher magnification images shown below. Scale bars of spinal cord cross sections represent 500 microns whereas they represent 200 microns in the higher magnification images shown below. Quantification of the intensity of staining is plotted in a scatter diagram. Statistical analysis was performed using Student's t-test and Welch correction. ***$p<0.001$; ****$p<0.0001$. Data are represented from 5 independent biological experiments. Error bar represents SEM.

Fig.6 Absence of CD4 results in severe poliomyelitis and dorsal root ganglionic inflammation during acute RSA59 infection. Sections of $CD4^{+/+}$ and $CD4^{-/-}$ mouse spinal cords were stained with H&E and immunohistochemically with anti-CD45. There is increased inflammation of the gray matter (poliomyelitis) and dorsal root ganglia in $CD4^{-/-}$ as compared

to $CD4^{+/+}$ mice. Mock-infected mice showed no inflammation. All scale bars indicate 90µm. N=5.

Fig.7 Absence of CD4 results in reduced viral clearance and altered expression of antiviral effector genes. a) Whole-brain lysates from $CD4^{+/+}$ and $CD4^{-/-}$ mice at days 5, 10 and 15 p.i. were subjected to comparative viral plaque assays on confluent monolayers of L2 cells. Each time point represents the mean titer for three mice. Titers are expressed as log10 PFU per gram of tissue. b) The relative abundance of transcripts corresponding to viral N-gene was compared using qRT-PCR in the $CD4^{+/+}$ and $CD4^{-/-}$ infected mouse brains at days 5, 10 and 15 p.i. c) Anti-N immunohistochemistry revealed the differential in-situ distribution of viral antigen in the representative anatomical regions (between brain stem and deep cerebellar white matter) of mock-infected $CD4^{+/+}$; and RSA59 infected $CD4^{+/+}$ and $CD4^{-/-}$ mice at days 6 and 30 p.i.. Scale bar 100µm (4X) and 50µm (40X). Relative gene expression of IFN γ (d), CXCL10 (e), TNFα (f) and CCL5 (g) at days 5, 10 and 15 p.i. were analyzed by qRT-PCR and compared between $CD4^{+/+}$ and $CD4^{-/-}$ mice. qRT-PCR results were expressed as fold mean ± SEM. Statistical analysis of the data represented in panels a, b, d, e, f, and g) was calculated using Two-way ANOVA, and multiple comparison was achieved by Hom's Sidak; *$p<0.05$; **$p<0.01$; ***$p<0.001$; ****$p<0.0001$. Data are represented from 3 independent biological experiments, N=3, 3 technical replicates each.

Fig.8 Absence of CD4 leads to severe chronic inflammatory demyelination and axonal loss. a) Cross-sections of $CD4^{+/+}$ and $CD4^{-/-}$ mouse spinal cords were analyzed for the presence of inflammatory lesions by H&E, demyelination by LFB, and inflammatory cells by anti-CD45 and anti-CD11b (microglia/macrophages) immunohistochemistry. Boxed areas are shown at higher magnification to right of the corresponding spinal cord cross sections. Arrows mark demyelinating plaques on the LFB stained sections, infiltrating inflammatory cells in the H&E stained sections, and immunoreactive leukocytes and microglia/macrophages in the CD45 and CD11b immunohistochemcally stained sections respectively. Scale bars of spinal cord cross sections represent 200 microns whereas they represent 50 microns in the higher magnification images. Levels of demyelination and inflammation are plotted in a scatter diagram (b, c, d). Statistical significance was calculated by unpaired Student's t-test and Welch correction. ***$p< 0.001$; ****$p<0.0001$). Data are represented from 4-5 independent biological experiments. Error bar represents SEM.

Fig.9 Absence of CD4 causes abnormal bulbar (brainstem) vacuolation and neuronal loss in RSA59 infected brains at day 30 p.i. a) Serial sagittal sections of brains from both $CD4^{+/+}$ and $CD4^{-/-}$ mice were analyzed for inflammation at day 30 p.i. by H&E and immunohistochemically by CD45 and CD11b. Boxed areas are shown at higher magnification below the corresponding brain midsagittal sections. Arrows mark infiltrating inflammatory cells in the H&E stained sections, and immunoreactive leukocytes and microglia/macrophages in the CD45 and CD11b immunohistochemcally stained sections respectively. Scale bars of spinal cord cross sections represent 200 microns whereas they represent 50 microns in the higher magnification images. Quantification of inflammation was performed for CD45 (b) and CD11b (c) staining. The level of significance was calculated by unpaired Student's t-test and Welch correction, ****$p<0.0001$). Error bar represents SEM. Data are represented from 4-5 independent biological experiments.

Fig. 10. Absence of CD4 causes no alteration in the axon-myelin coherence in the brain stem and spinal cord of mock infected mice. Toluidine blue stained sections of glutaraldehyde fixed, epoxy resin embedded sections (500 nm thick) from mock infected $CD4^{-/-}$ mouse brain stem (A, B) and spinal cord (C, D). A. Gray and white matter of brain stem. Arrows mark bundles of intact myelinated fibres. Asterisks mark the neuronal nuclei. Original magnification – 400X. B. Brain stem white matter. Original magnification - 1000X. C. Spinal cord cross section. Original magnification 40X. Posterior columns in boxed area are further magnified in D. Original magnification 1000X. White and gray matter in both the brain stem and spinal cord show no evidence of inflammation, demyelination or cellular injury.

Fig.11 Absence of CD4 results in severe spinal cord axonal injury upon RSA59 infection at the chronic stage. a and b: Toluidine blue-stained sections. a) Posterior columns (200X) and b) (1000X) demonstrate clusters of degenerating axons. Arrows - degenerating axons, asterixes - swollen myelin sheaths. c and d: Corresponding electron microscopy. c) Swollen myelin sheaths with loss of axoplasm (7,500X). d) Cluster of degenerating axons with collapsed myelin sheaths (10,000X). The arrow shows the corresponding area on the toluidine blue-stained section. Scale bar represents 2 microns. Data are represented from 3 independent biological experiments.

Fig.12 qRT-PCR analysis of IL-6, IL-10, CD86, Btk and CD163 reveals an inflammatory state in the brains of RSA59 infected $CD4^{-/-}$ mice. Quantitative PCR analysis of IL-6 (a) IL-10 (b); CD86 (c); Btk (d); CD163 (e) analysis was performed in RSA59 infected $CD4^{+/+}$ and

$CD4^{-/-}$ mouse brains at days 5, 10 and 15. Data are represented from 3 independent biological experiments, N=3, 3 technical replicates each. Statistical analysis was performed by Two-way ANOVA, Hom Sidak's multiple comparison test; **p<0.01; ***p<0.001; ****p<0.0001. Error bar represents SEM.

Table I. Average Inflammation score in RSA59-infected $CD4^{+/+}$ and $CD4^{-/-}$ mouse brain (47)

	No. of mice	No. of sections	% mice with inflammation	Mean score of Inflammation (mean ± SEM)
Acute phase RSA59 $CD4^{+/+}$	4	08	100 %	1.8±0.322
Chronic phase RSA59 $CD4^{+/+}$	5	10	100 %	1.4±0.163
Acute phase RSA59 $CD4^{-/-}$	4	08	100%	2.0±0.189
Chronic Phase RSA59 $CD4^{-/-}$	4	10	100%	2.5±0.189

Significant difference was observed only at the chronic phase of infection between $CD4^{+/+}$ and $CD4^{-/-}$ brains (***p=0.0004)

Table II. Average Inflammation score in RSA59-infected $CD4^{+/+}$ and $CD4^{-/-}$ mouse spinal cord (47)

	No. of mice	No. of sections	% mice with inflammation	Mean score of Inflammation (mean ± SEM)
Acute phase RSA59 $CD4^{+/+}$	3*	20	80 %	0.6±0.112
Chronic phase RSA59 $CD4^{+/+}$	5	30	100 %	0.76±0.114
Acute phase RSA59 $CD4^{-/-}$	4	20	100%	1.1±0.143
Chronic Phase RSA59 $CD4^{-/-}$	4	20	100%	1.05±0.05

*1 mouse was an outlier; it did not get infected.

Table III. List of Primers

Gene	Forward 5'-3'	Reverse 5'-3'
CD86	GGCTCAAAACATAAGCCTGA	CCCATGTCCTTGATCTGAAC
CD163	GAGACACACGGAGCCATCAA	TGGACAAACCTTTTACAACCAGG
IFN γ	GTCTCTTCTTGGATATCTGGAGGAACT	GTAGTAATCAGGTGTGATTCAATGACGC
TNF α	CTGTAGCCCACGTCGTAGC	TTGAGATCCATGCCGTTG
CCl5	CCA ATC TTG CAG TCG TGT TTGT	CAT CTC CAA ATA GTT GAT GTA TTC TTG AAC
CXCL10	GACGGTCCGCTGCAACTG	CTTCCCTATGGCCCTCATTCT
Btk1	ACAGCAGAACACATTGCTCA	GGGAACTCCTCAGGAAACAT
IL12 p40	GGAAGCACGGCAGCAGAATA	AACTTGAGGGAGAAGTAGGAATGG
IL6	AGTTGCCTTCTTGGGACTGA	TCCACGATTTCCCAGAGAAC
IL10	AGTGGAGCAGGTGAAGAGTG	TTCGGGAGAGGTACAAACG
Anti -N	AGGATAGAAGTCTGTTGGCTCA	GAGAGAAGTTAGCAAGGTCCTACG
GAPDH	GCCCCTTCTGCCGATGC	CTTTCCAGAGGGGCCATCC
B- Actin	CTTCTACAATGAGCTGCGTGTG	GGTCTCAAACATGATCTGG

890

891

Chakravarty et. al., Fig. 1

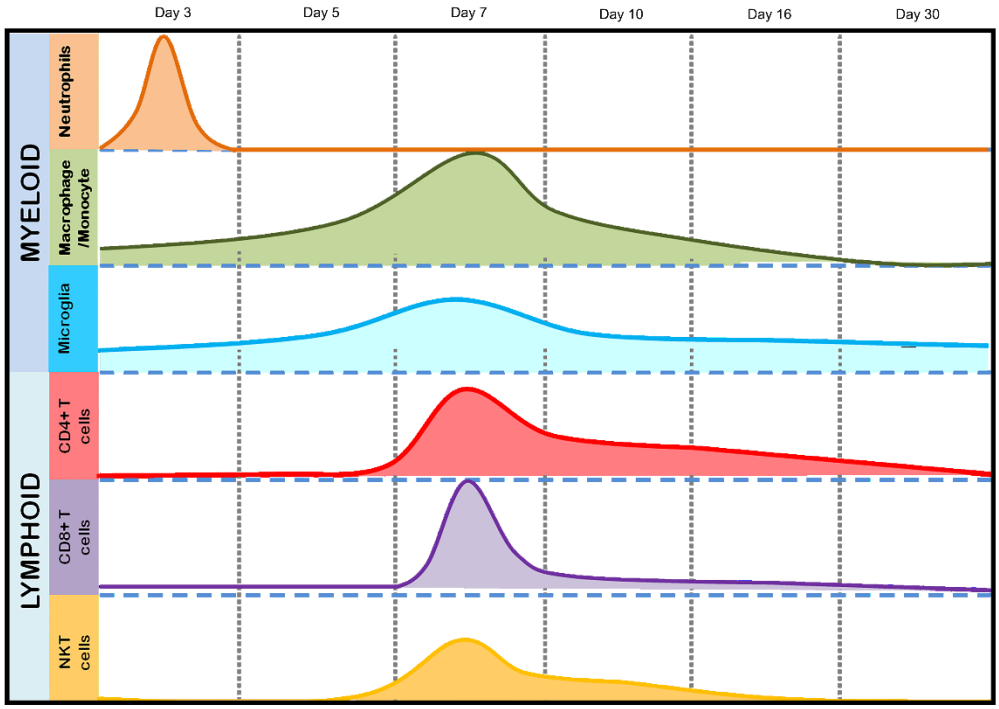

892

893

894

895

896

897

898

899

900

901

902

903

Chakravarty et. al., Fig. 2

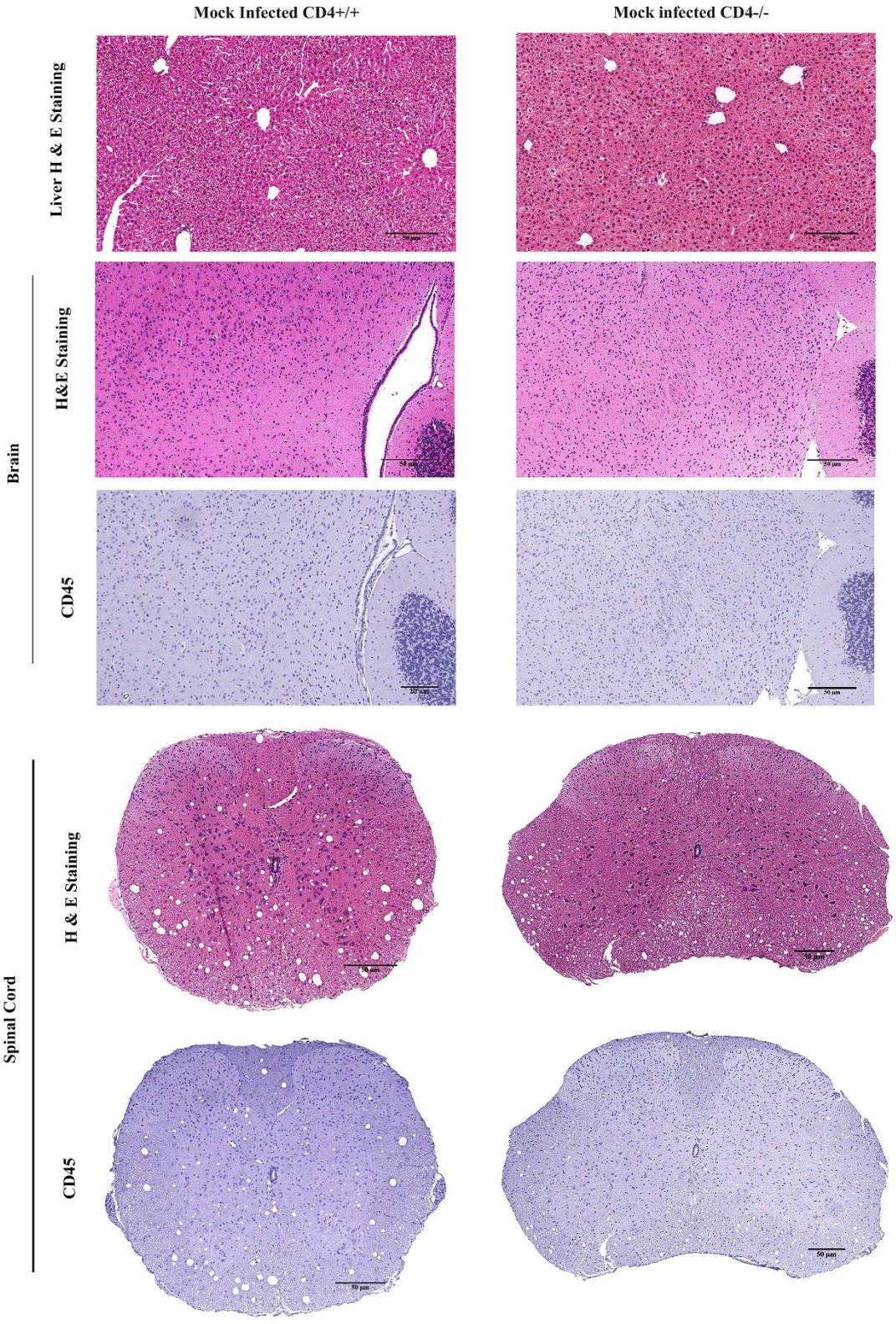

904

905

Chakravarty et. al., Fig 3

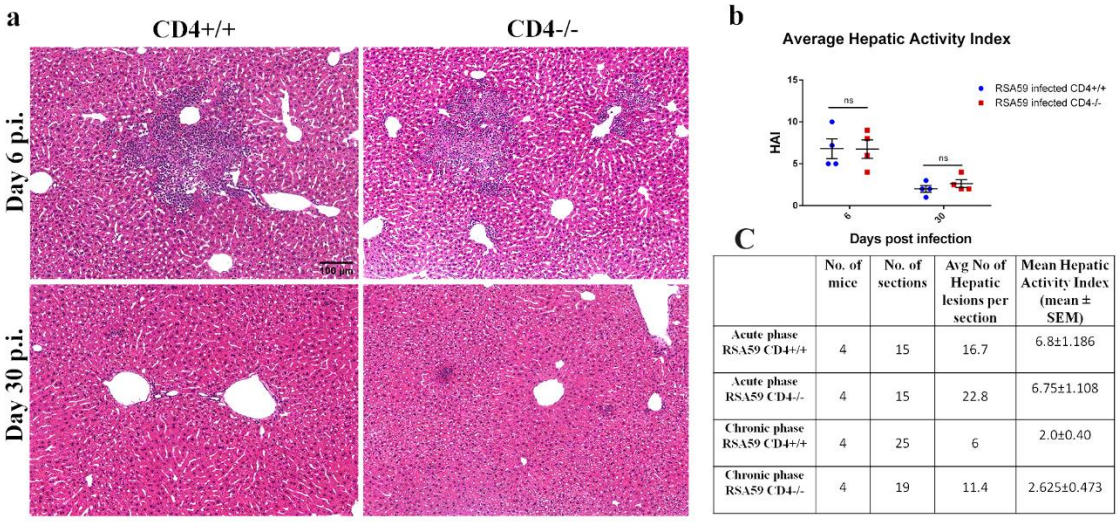

C

	No. of mice	No. of sections	Avg No of Hepatic lesions per section	Mean Hepatic Activity Index (mean ± SEM)
Acute phase RSA59 CD4+/+	4	15	16.7	6.8±1.186
Acute phase RSA59 CD4-/-	4	15	22.8	6.75±1.108
Chronic phase RSA59 CD4+/+	4	25	6	2.0±0.40
Chronic phase RSA59 CD4-/-	4	19	11.4	2.625±0.473

Chakravarty et. al., Fig. 4

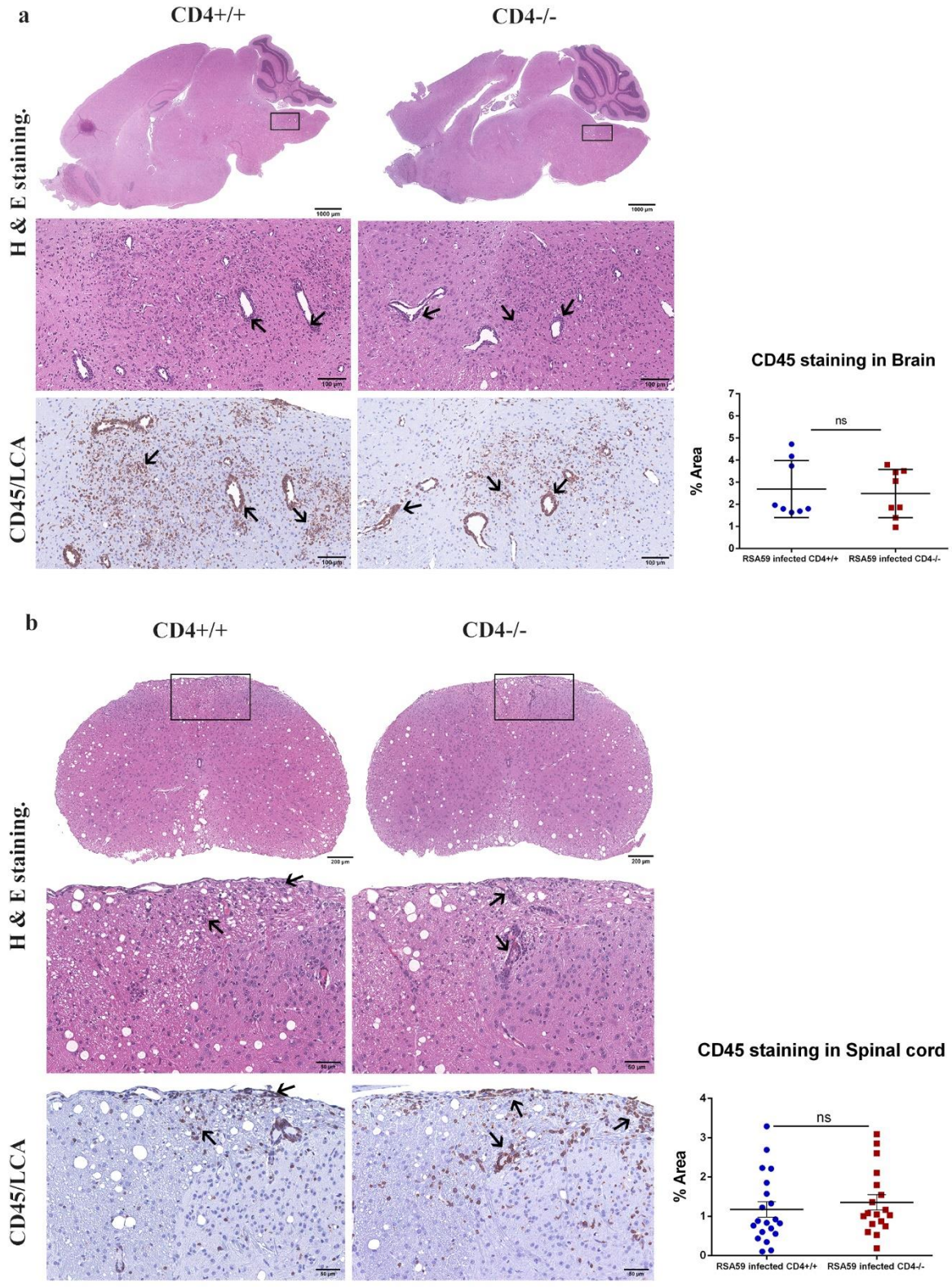

Chakravarty et. al., Fig. 5

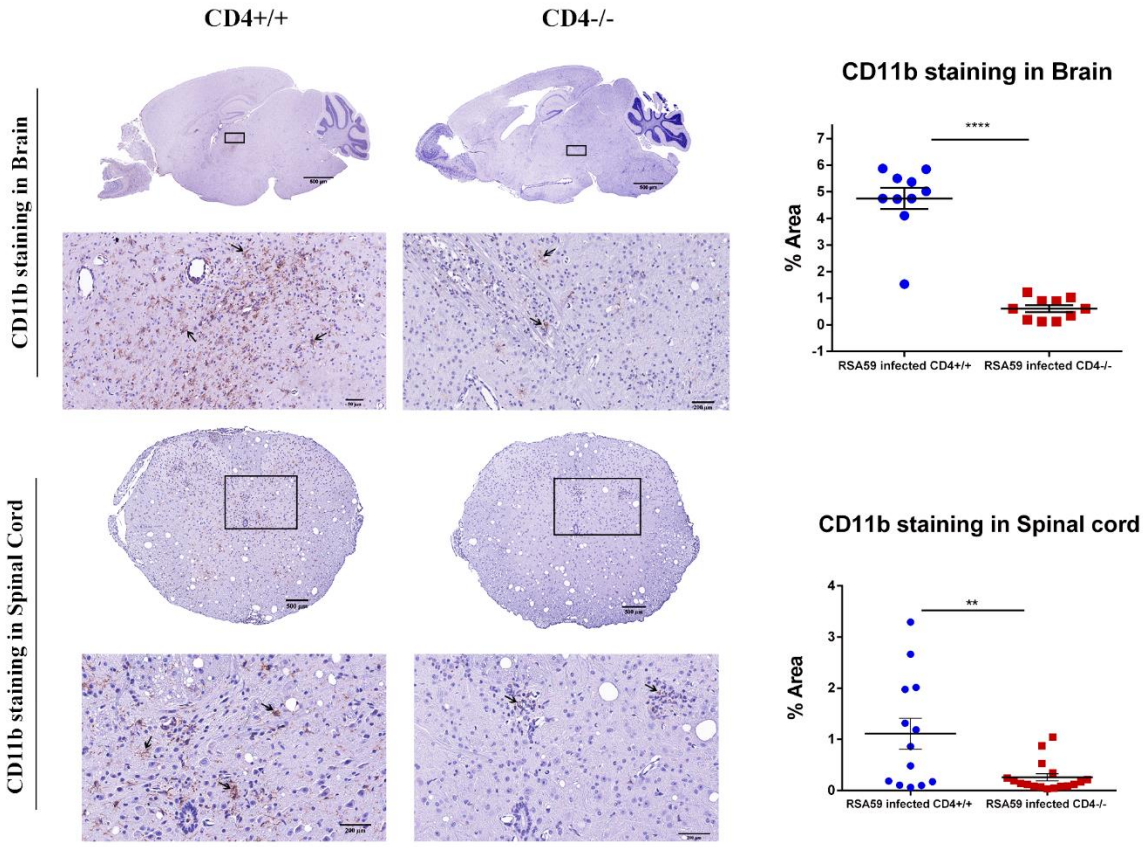

923

924

925

926

927

928

929

930

931

Chakravarty et. al., Fig. 6

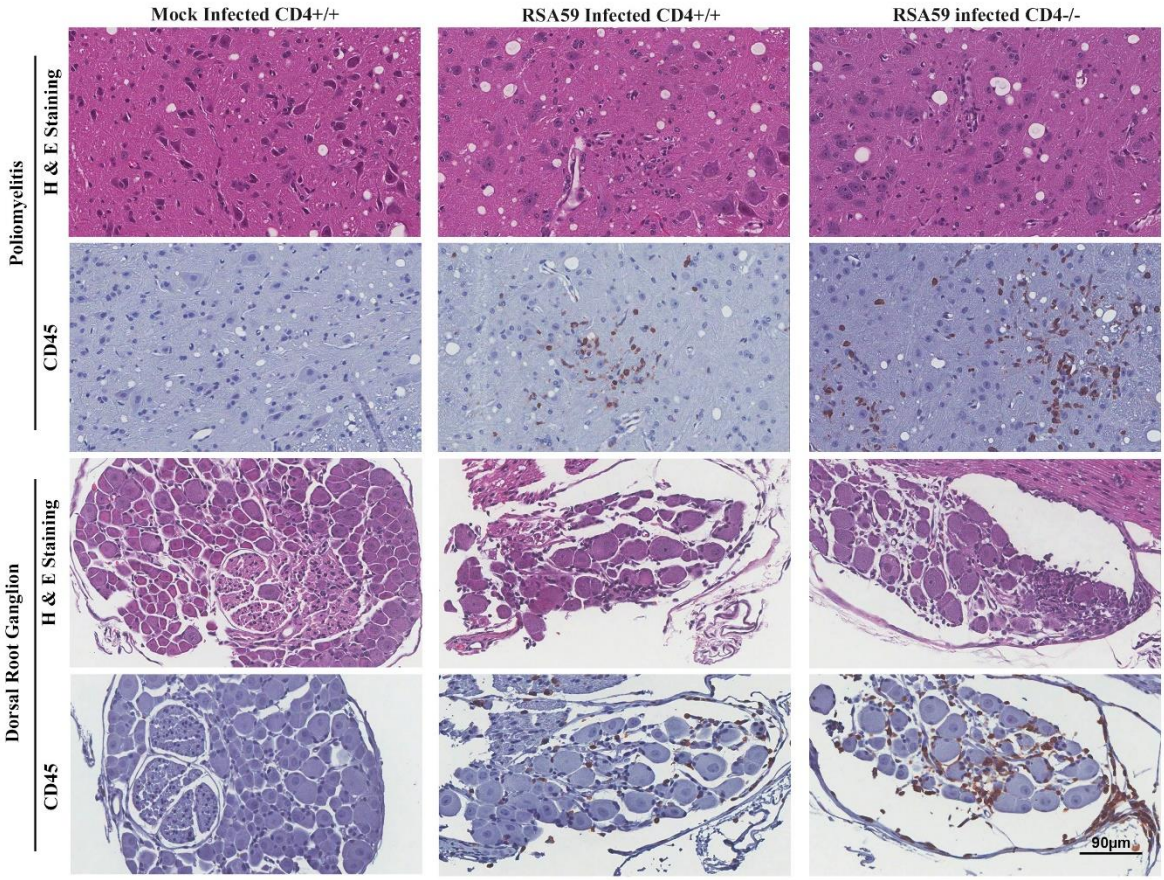

Chakravarty et. al., Fig. 7

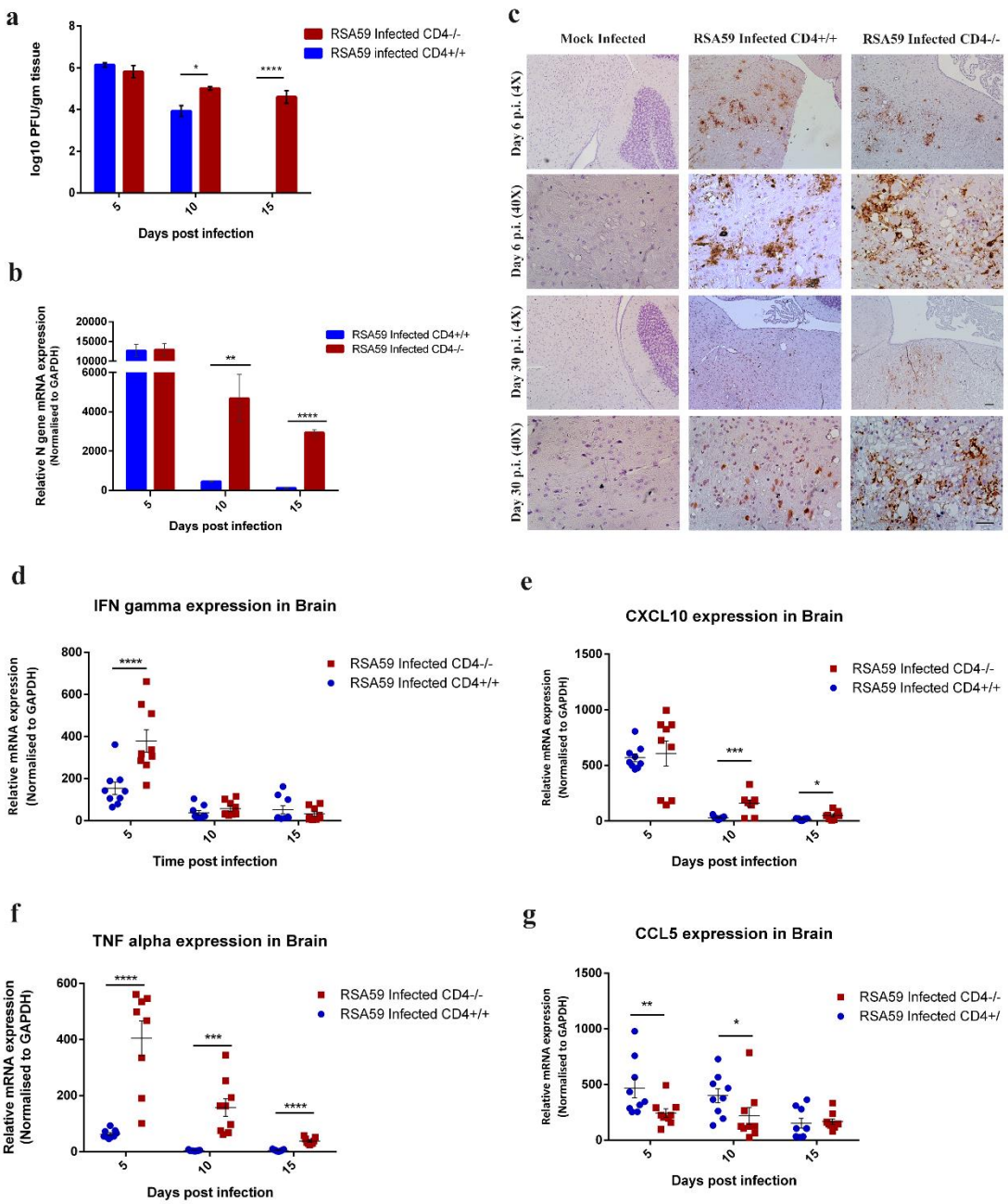

Chakravarty et. al., Fig. 8

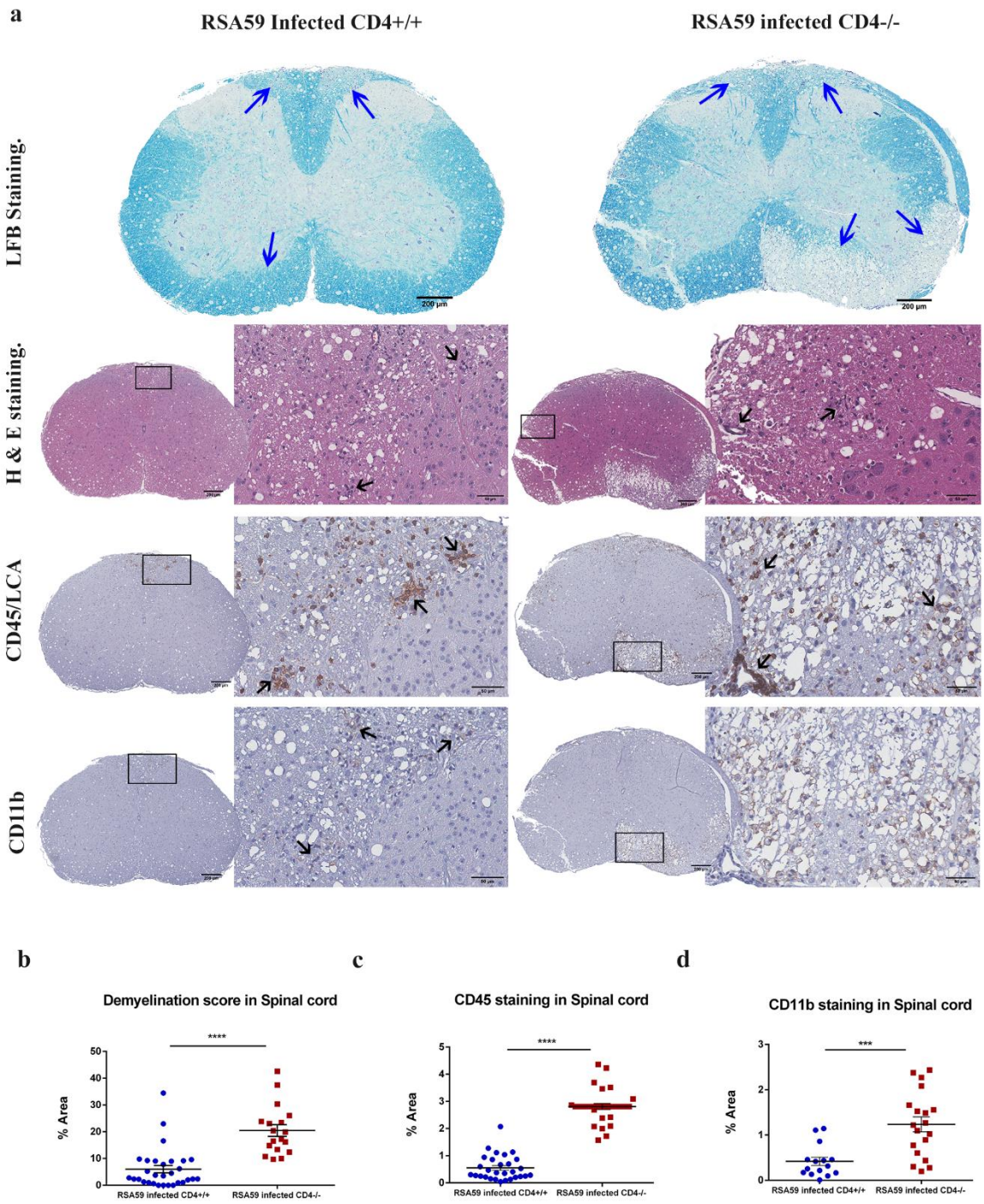

946

947

948

Chakravarty et. al., Fig. 9

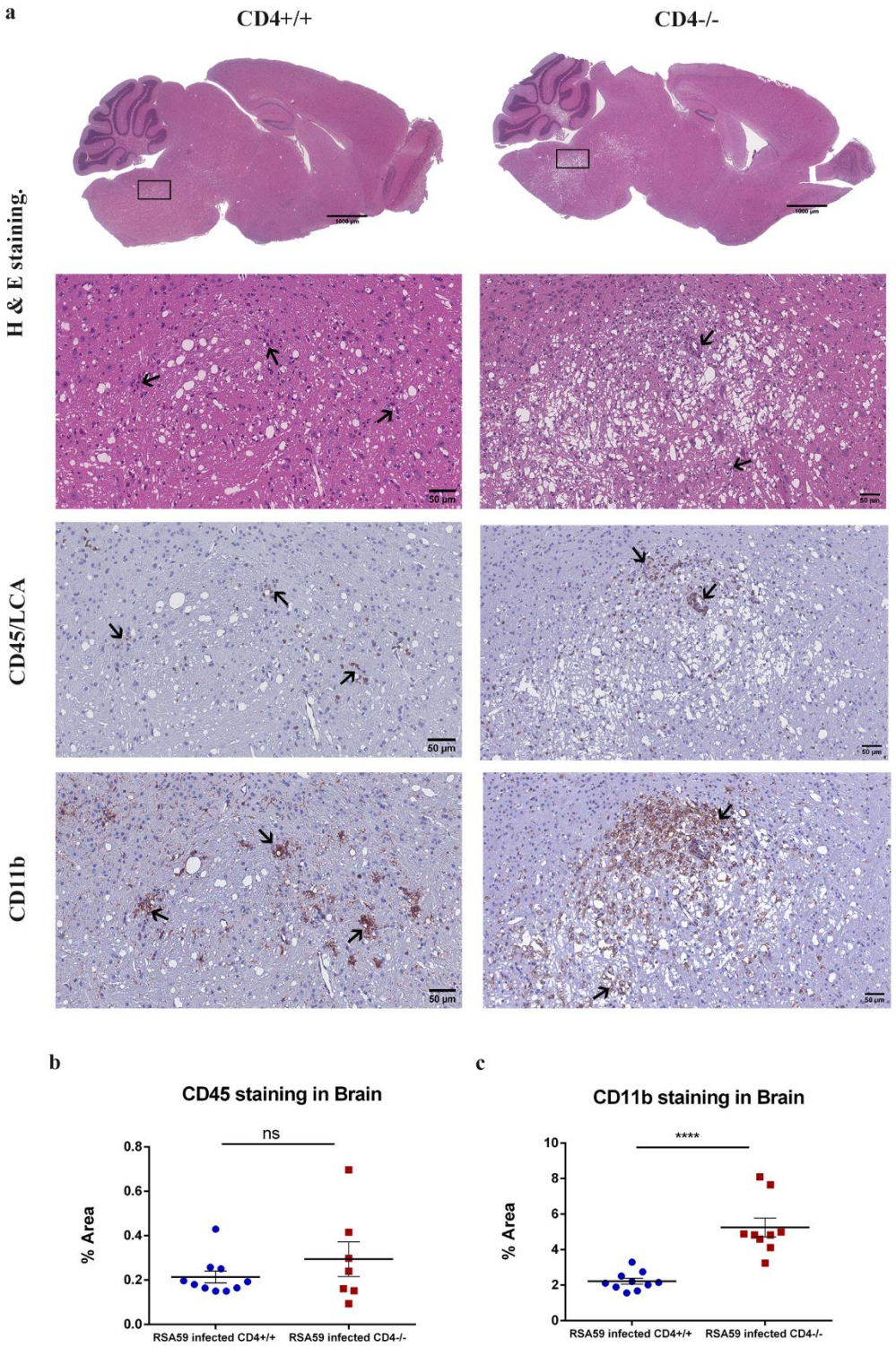

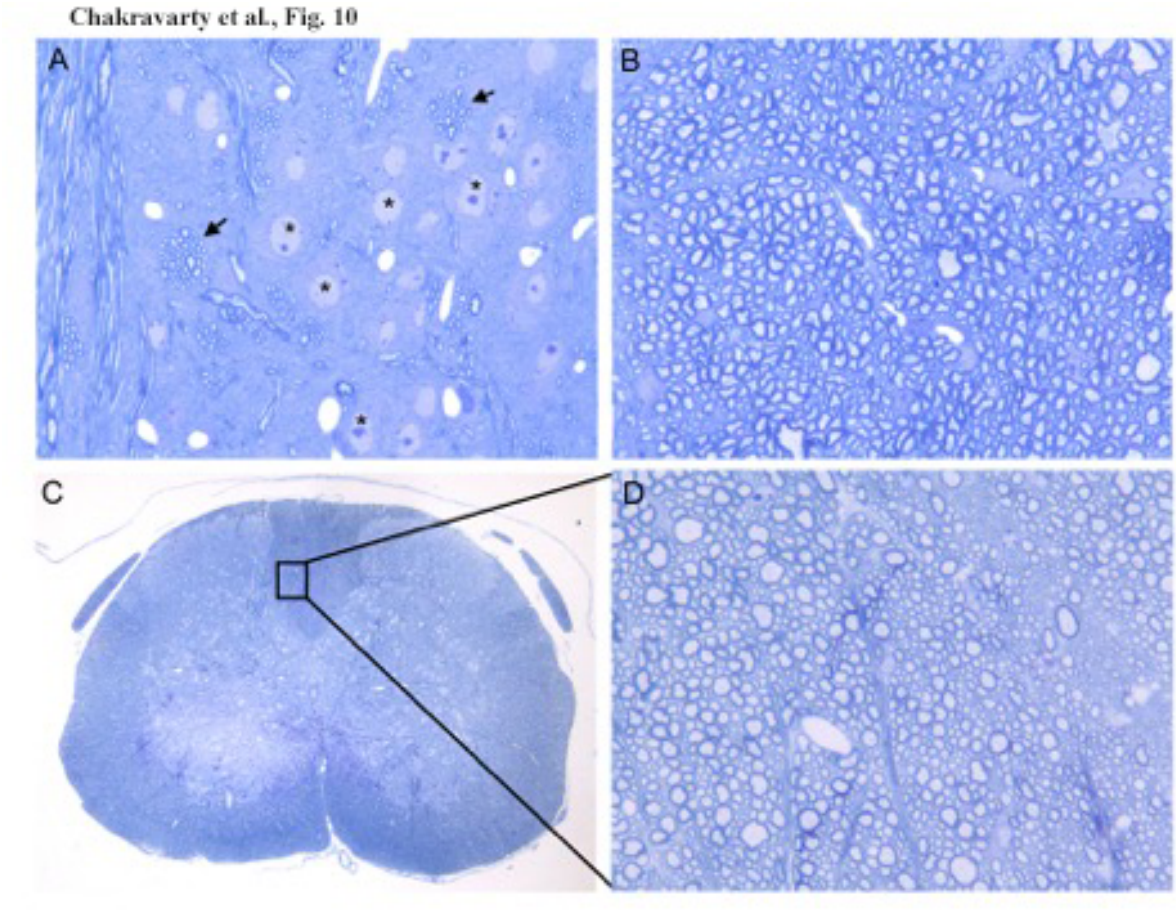

952

953

954

955

956

957

958

959

960

961

962

Chakravarty et al., Fig. 11

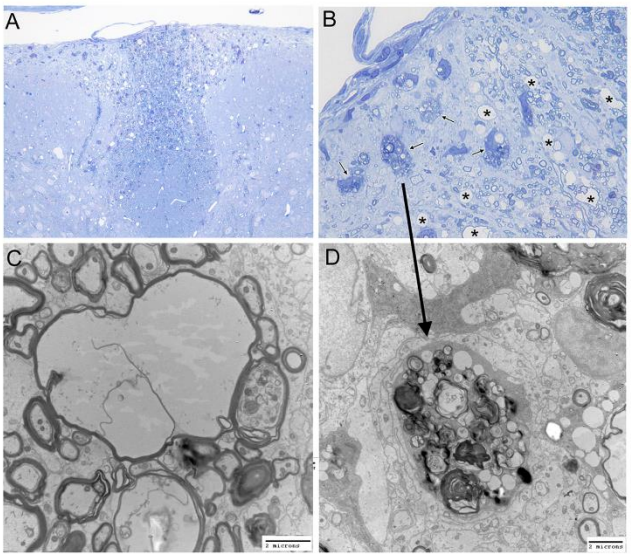

963

964

965

Chakravarty et al., Fig. 12

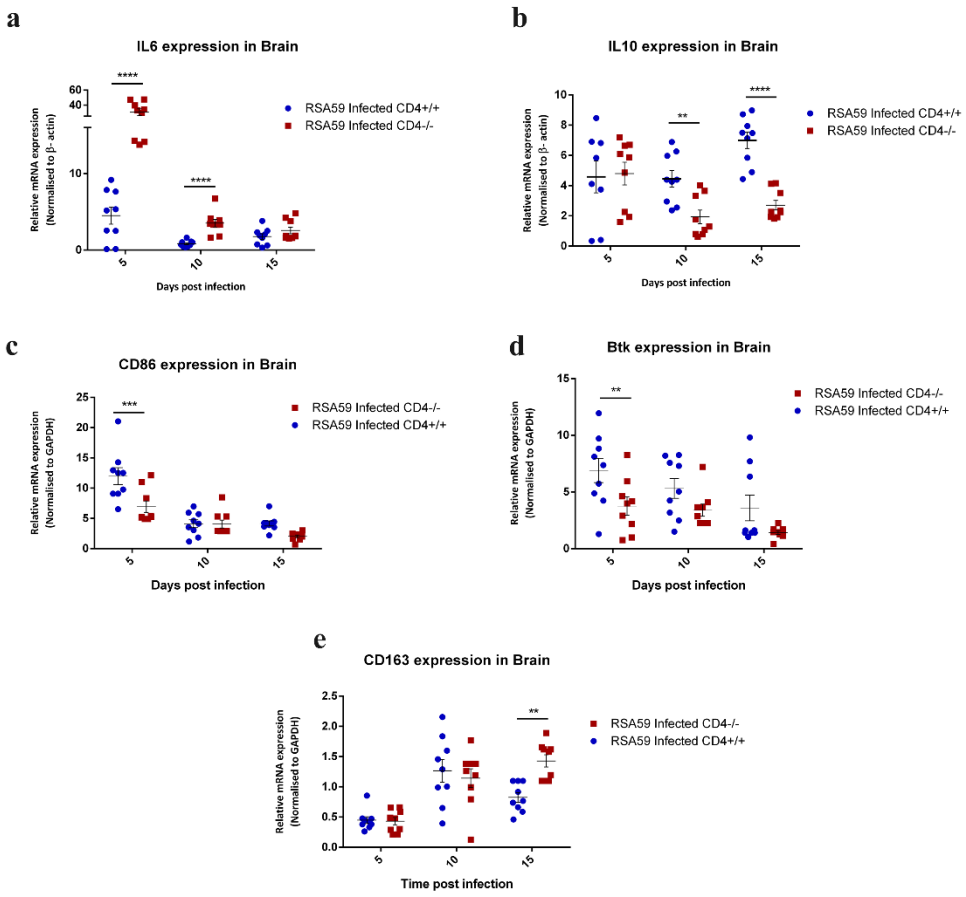

966

967

968

969

970

971

972

973

974

975

976

977